

1 **Planning and Implementation of the Tropical Composition, Cloud and Climate Coupling** 2 **Experiment (TC4)**

3
4 Owen B. Toon¹, David O. Starr², Eric J. Jensen³, Paul A. Newman², Steven E. Platnick², Mark R.
5 Schoeberl², Paul O. Wennberg⁴, Steven C. Wofsy⁵, Michael J. Kurylo⁶, Hal Maring⁷, Kenneth
6 W. Jucks⁷, Michael S. Craig³, Marilyn F. Vasques³, Lenny Pfister³, Karen Rosenlof⁸, Henry B.
7 Selkirk⁶, Peter R. Colarco², Stephan R. Kawa², Gerald G. Mace⁹, Patrick Minnis¹⁰, Kenneth E.
8 Pickering²

9
10
11 ¹ University of Colorado, Boulder, Colorado, USA.

12 ² NASA Goddard Space Flight Center, Greenbelt, Maryland, USA.

13 ³ NASA Ames Research Center, Moffett Field, California, USA.

14 ⁴ California Institute of Technology, Pasadena, California, USA.

15 ⁵ Harvard University, Cambridge, Massachusetts, USA.

16 ⁶ Goddard Earth Sciences and Technology Center, Greenbelt, MD, USA

17 ⁷ NASA Headquarters, Washington, D.C., USA

18 ⁸ NOAA Earth System Research Laboratory, Boulder, Colorado, USA

19 ⁹ University of Utah, Salt Lake City, Utah, USA

20 ¹⁰ NASA Langley Research Center, Hampton, Virginia, USA.

21 22 **Abstract**

23 We describe the scientific motivation behind the Tropical Composition, Cloud and Climate
24 Coupling Experiment, (TC4), which was based in Costa Rica and Panama during July and
25 August 2007. We then discuss the various flights that took place and summarize the initial
26 results from TC4. Significant progress was made in understanding the radiative properties of
27 anvils and other tropical cirrus, the mechanisms and modes of transport of air into the
28 stratosphere, and the chemistry of the tropical atmosphere.

29 30 **1. Introduction**

31
32 The Tropical Composition, Cloud and Climate Coupling Experiment, (TC4), was based in
33 Costa Rica and Panama during July and August 2007. The more than 600 participants came
34 from multiple NASA centers, NOAA, NCAR, numerous universities, private research
35 institutions, Panama and Costa Rica. The field mission involved the NASA DC-8, ER-2 and
36 WB-57F aircraft (Figure 1) as well as ground based instruments and sondes. The mission was
37 aimed at better understanding the Tropical Tropopause Layer (TTL) by combining in situ and
38 remotely sensed data from the ground, balloons, and aircraft with data from NASA satellites
39 such as Aura, CloudSat, CALIPSO, Aqua, and Terra. The TTL is of critical importance to the
40 Earth's climate and atmospheric chemistry because it is the gateway to the stratosphere. Deep
41 convection sometimes penetrates the TTL to reach the stratosphere, while gentle upward motions
42 within the TTL may also loft materials across the tropical tropopause. Hence the chemistry of
43 the stratosphere, including the global ozone budget, may be affected in a significant way by
44 processes that alter the transport across the TTL and by the chemicals in the TTL. Changes in
45 water vapor in the stratosphere and upper troposphere can play an important role in modulating
46 the climate since water is the most powerful greenhouse gas in the atmosphere. The TTL is the

47 main dehydration region for air entering the stratosphere, and it is also an important reservoir for
48 moisture lofted by tropical convection. Understanding how water behaves in the TTL is one key
49 to better understanding the greenhouse effect, and global climate change. The TTL also contains
50 cirrus clouds. One type of cirrus consists of anvils, the flattened tops of tropical cumulus clouds.
51 In just a few minutes, a cumulus cloud can pump vast quantities of air from near the tropical
52 surface to the TTL, where the air spills out into the anvils. The TTL also contains cirrus clouds
53 that form in situ. Some of these are so thin that they cannot be seen with the naked eye, and so
54 are called sub-visible cirrus. These clouds are easily detected by some satellites, however, and
55 are now known to cover a large fraction of the tropics.

56 Here we provide an overview of the TC4 mission. We first describe the goals for TC4. We
57 then discuss the instrument packages on the aircraft and other platforms. Next, we summarize
58 the various flights that were conducted. Finally, we provide an overview of the results from TC4
59 to date.

60

61 **2. Scientific Motivation**

62

63 Table 1 lists the major questions that TC4 sought to address. The focus of TC4 was the
64 TTL. However, TC4 recognized that an understanding of the flux of material into the TTL
65 requires constituent measurements throughout the troposphere, including convectively disturbed
66 regions. An understanding of the role of water vapor and ozone in the climate system requires
67 observations below the lower boundary of the TTL in the free troposphere. Similarly,
68 measurements in the lower stratosphere are required to understand how processes in the TTL
69 influence humidity and other properties of the stratosphere. Below we address a number of
70 issues related to the questions in Table 1.

71

72 **2.1. Definition of the TTL**

73

74 A number of workers have noted that the layer of the tropical atmosphere between about 12
75 km altitude (pressure~200 hPa , potential temperature, θ , ~350 K) and the cold point tropopause
76 (16–17 km, 100–90 hPa, $\theta \sim 380$ K) has characteristics intermediate between those of the
77 troposphere and stratosphere (e. g. *Highwood and Hoskins [1998], Thuburn and Craig [2002],*
78 *Fueglistaler et al., 2008*]). This layer was referred to as the *substratosphere* by Thuburn and
79 Craig. The cold point tropopause (altitude of the temperature minimum) is important for
80 understanding stratospheric dehydration, and for infrared radiative forcing, but it is not a material
81 surface. In fact, some tropospheric circulations (such as overshooting convection, monsoon
82 circulations, and equatorial waves) can extend for some distance above the cold point
83 tropopause. Thus, it seems appropriate to extend the definition of the transition layer between
84 the tropical troposphere and stratosphere to include the first few kilometers above the cold point.
85 Therefore this region is referred to as the Tropical Tropopause Layer (TTL) rather than the
86 substratosphere. The TTL as defined here includes the entire region between the level at which
87 the temperature profile begins to depart from the moist adiabatic profile enforced by tropospheric
88 convection (~12 km in convectively active regions *Gottelman and Forster [2002]*) to the level in
89 the stratospheric overworld beyond which the influence of tropospheric circulations becomes
90 insignificant (~50 hPa, ~20 km, $\theta \sim 470$ K). The stratospheric overworld is defined to be the
91 volume of the stratosphere with potential temperature above the mean tropical tropopause

92 potential temperature, $\theta \sim 380\text{K}$. At middle latitudes there is a lower stratosphere with potential
93 temperatures characteristic of the tropical troposphere.

94 Within the TTL, as defined above, a number of parameters undergo rapid change in the
95 vertical. For example, in the lower portion of the TTL ($\sim 12\text{--}14\text{ km}$) convective mass fluxes (and
96 clear sky radiative cooling rates) decrease rapidly with height, corresponding to the level of the
97 main convective outflow. The annual mean convective mass flux out of the boundary layer
98 between 15°N and 15°S is about $3.0 \times 10^{11}\text{ kg/s}$, and about 50% of this mass flux from the
99 boundary layer reaches the base of the TTL. However, the annual flux across the 100 hPa
100 surface (near the coldpoint) is only about 10^{10} kg/s , which is only $\sim 3\%$ of the flux of air out of
101 the tropical boundary layer [Rosenlof and Holton, 1993]. There are also vertical variations in the
102 horizontal transport, and above 14 km, where convective transport and mixing are small, large-
103 scale horizontal transport processes become increasingly important for meridional transport and
104 mixing of trace constituents. A layer extending from approximately 15.5 km into the lowermost
105 stratosphere is (at least in clear-sky conditions) radiatively heated [Gettelman *et al.*, 2004]. In
106 balance with this heating, air in this layer must be ascending and will ultimately end up in the
107 stratosphere. As a result, the composition of the TTL represents a lower boundary condition for
108 important trace gases that affect stratospheric ozone, including water vapor, HO_x and NO_x
109 species, and halogens. The TTL is also a region in which relative humidity increases with
110 altitude, with a maximum at the tropopause (Vömel *et al.*, 2002).

111 In addition, while it is known that photochemistry within the TTL leads to rapid ozone
112 production, the interplay of the convective processes (that transport short-lived compounds that
113 fuel ozone production from the lower troposphere), in situ photochemistry, and large scale
114 dynamics remains poorly constrained.

115 The transport and transformations within the TTL are also important for understanding the
116 fate of compounds transported into the tropical upper troposphere and the chemical boundary
117 condition for the stratosphere. The above estimates of mass fluxes indicate that only a small
118 fraction of the air leaving the tropical boundary layer actually crosses into the tropical
119 stratosphere. For short-lived or soluble constituents, the fraction reaching the stratosphere will be
120 even smaller. However, these estimates are very uncertain and the flux of compounds into the
121 stratosphere will depend on the precise balance of different physical and chemical processes in
122 the TTL. Better quantification of these processes is essential for establishing the chemical
123 boundary condition for the stratosphere, and understanding how this will change.

124 Figure 2 presents three visions of transport from the troposphere into the lower stratosphere.
125 On the left side of the figure the green cumulus has a turret overshooting the cold point
126 tropopause. In this model, which has dominated thinking since the 1980s, air moves from the
127 ground to the stratosphere in tens of minutes. The overshooting turret leaves dehydrated air
128 behind in the stratosphere because the ice in the turret falls out too fast to evaporate in the
129 stratosphere. It now appears that such over shooting convection does occur, but is rare in the
130 tropics, and that such clouds generally hydrate the air, and only dehydrate if the air surrounding
131 the turret is already supersaturated [Liu and Zipser, 2005; Corti *et al.*, 2008, Jensen *et al.*, 2007]
132 The yellow cumulus clouds in Figure 2 represent the ideas of Corti *et al.* [2006]. These clouds
133 detrain between about 12 and 15 km, with the most likely location being about 13 km, just a
134 kilometer above the ceiling of the NASA DC-8. Air can reach these levels from the boundary
135 layer in tens of minutes given the large vertical velocities in convective cores. The air detrains
136 from the cores, and the anvil cloud can spread for several hours. If the ice in the anvil evaporates
137 or falls out of the air parcel, the air parcel will radiatively cool and begin to descend. Corti *et al.*

138 [2006] found that this descent is rapid. On the other hand, air parcels that retain ice will be
139 radiatively heated and ascend. In about two weeks the parcels may have ascended to high
140 enough altitudes to reach about 16 km, where clear sky radiative heating can slowly drive them
141 across the tropopause. The third view in Figure 2 is represented by the red subvisible cirrus. In
142 models suggested by *Jensen et al.* [1996], *Hartman et al.* [2001] and *Holton and Gettelman*
143 [2001] among others, it is assumed that convection hydrates the air below the tropopause.
144 However, whenever the air moves horizontally into cold regions, cirrus clouds will form and
145 dehydrate the air. The last step in this process occurs when air near the tropopause cools either
146 due to vertically propagating waves, or due to horizontal transport into cold regions. Then
147 subvisible cirrus form in situ, dehydrating the air mass, and vertical motions driven by radiative
148 heating in the subvisible cirrus drives the dehydrated air into the stratosphere.

149

150 **2.2. The TTL water vapor budget**

151

152 A great deal of attention has been focused on processes controlling the TTL water vapor
153 budget and the H_2O concentration of air entering the stratosphere (H_2O_{entry}). Several studies
154 have shown that cirrus formed in situ within the TTL can freeze dry air ascending through the
155 cold tropopause region, reproducing observed water vapor concentrations, including interannual
156 variability [e.g. *Gettelman et al.*, 2002; *Jensen and Pfister*, 2004; *Fueglistaler and Haynes*,
157 2005]. Both vertical and horizontal transport are important in determining H_2O_{entry} ; horizontal
158 transport in the TTL is very rapid while vertical transport is slow (it takes on the order of a few
159 months for air parcels to ascend from 360 K to 390 K potential temperature, see Figure 2)
160 [*Holton and Gettelman*, 2001]. To first order, the H_2O_{entry} will be controlled by the minimum
161 temperatures encountered by air parcels in their journey upward through the TTL. This assertion
162 is supported by the correspondence between a recent decrease in lower-stratospheric humidity
163 and the decrease in tropical tropopause temperatures [*Randel et al.*, 2004]. However, as
164 discussed below, TTL cirrus clouds do not necessarily remove all vapor in excess of saturation,
165 and details of the cloud microphysical properties and interactions with water vapor are important
166 for understanding the dehydration process.

167 The role of deep convection in the upper troposphere/lower stratosphere (TTL) water vapor
168 budget is less well understood than the role of cirrus in removing water. Deep convection is
169 certainly a source of water vapor and ice clouds to the TTL, and it is well established that
170 extreme convective events can overshoot well into the stratosphere, resulting in local hydration
171 events [*Liu and Zipser*, 2005; *Corti et al.*, 2008]. It also appears likely that convective injection
172 of ice into the often ice-supersaturated TTL can result in dehydration events [*Jensen et al.*,
173 2007]. Modeling studies have shown that convective injection throughout the TTL is required to
174 explain observed concentrations of water vapor isotopes [*Dessler et al.*, 2007]. However, the
175 overall impact of convection on water vapor abundance in the TTL remains poorly quantified.

176

177 **2.3. Tropical clouds**

178

179 Recent studies have shown that the response of surface temperature to increasing
180 greenhouse gas concentrations depends sensitively on the processes controlling tropical cirrus
181 anvil production. As greenhouse gases drive up the sea surface temperature, convection may
182 become more intense. However, it is not clear that increased convective intensity implies larger,

183 longer-lived cirrus anvils. In stronger convective systems, the removal of water by droplet and
184 ice crystal precipitation may be more efficient, resulting in decreased ice mass outflow into the
185 anvil. Evaluation of this sensitivity using satellite data has proven challenging because of
186 problems determining convective intensity and cirrus anvil properties from satellite
187 measurements. Also, local compensating subsidence may be appreciably enhanced which might
188 also decrease cirrus lifetime and extent. A recent study that combined ground-based cloud radar
189 observations with geostationary satellite-derived trajectories [Mace *et al.*, 2005] found evidence
190 that tropical cirrus properties did vary when cirrus were observed to originate from convection
191 near large western Pacific Islands compared to cirrus from purely maritime sources. Using
192 TRMM data, the properties of the former population of clouds were derived from convection that
193 tended to be more intense, and these clouds tended to have higher concentrations of smaller
194 particles.

195 TC4 sought to improve understanding of the processes controlling the cirrus anvil
196 production and evolution. These processes include the dynamics of the convection and the
197 outflow anvil, cloud microphysics (droplet activation, ice crystal nucleation, coalescence,
198 precipitation, etc.), and interactions between dynamics, microphysics, and radiation. These case-
199 study modeling efforts will serve both to improve the detailed cloud models and to provide
200 insights for development of GCM cloud parameterizations.

201 It should be noted that there have been several previous studies in the tropics related to deep
202 convection. For instance, the 1974 Global Atmospheric Research Program Atlantic Tropical
203 Experiment (GATE), the 1992-1993 Tropical Ocean Global Atmosphere Coupled Ocean
204 Atmosphere Response Experiment (TOGA-COARE), and the 1993 Central Equatorial Pacific
205 Experiment (CEPEX) all investigated the role of convection in the tropical energy budget. The
206 1984 Stratospheric Troposphere Exchange Project (STEP) on the other hand investigated the role
207 of convection in transporting water vapor into the stratosphere. TC4 brought new instruments to
208 bear on some of these issues, but also had different goals. For example, TC4 measured the
209 properties of tropical marine anvils in detail, which was not done in the previous tropical
210 missions, but was done in tropical continental anvils in a TC4 predecessor mission the 2002
211 Cirrus Regional Study of Tropical Anvils and Cirrus Layers - Florida Area Cirrus Experiment
212 (CRYSTAL-FACE). TC4 also investigated the role of sub-visible cirrus in exchange between
213 the stratosphere and troposphere, as did its predecessor mission, the 2006 Costa Rica-Aura
214 Validation Experiment CR-AVE. STEP, CRYSTAL-FACE and CR-AVE are outlined at
215 <http://www.espo.nasa.gov/missions.php>.

216 In addition to convective intensity, anvil properties can also be impacted by the aerosols
217 which form nuclei to activate the water droplets at the base of clouds, heterogeneous nuclei
218 which may lead to freezing inside clouds, or heterogeneous nuclei which may lead to particle
219 formation in the anvils, or in other types of cirrus. Data collected in CRYSTAL FACE indicated
220 a connection between the anvil properties and the aerosols in the boundary layer and in the free
221 troposphere (eg., Fridlind *et al.* [2004], DeMott *et al.* [2003]).

222 In addition to investigating cirrus anvil production processes, TC4 planned to improve
223 understanding of cirrus anvil evolution processes. The coverage of cirrus in the tropics depends
224 on anvil lifetimes and the conversion of anvil outflow into self-maintaining cirrus layers. Luo
225 and Rossow [2004] and Mace *et al.* [2005] show that a substantial portion of tropical cirrus is not
226 directly associated with deep convection. While it is known that solar and infrared radiative
227 heating in cirrus anvils can drive thermal instability and small-scale convection within the anvils,
228 it is not known to what extent other factors such as a high background humidity or large scale

229 vertical motion contribute to tropical cirrus longevity. Factors likely to affect cirrus longevity
230 include upper tropospheric humidity, large-scale dynamics, and wind shear, which in turn may
231 be driven by radiative forcing impacted by cirrus. Extremely strong convective systems can
232 generate cirrus with tops in the highest few kilometers of the troposphere. The final stage of
233 these very high cirrus is unclear. As the larger ice crystals fall out, leaving behind optically thin
234 cirrus, the clouds may be lofted by radiative heating, resulting in persistent thin cirrus as often
235 observed near the tropopause.

236 Tropical cirrus clouds are also frequently observed in locations remote from deep
237 convection, perhaps existing as remnants of convective storms or perhaps formed by other
238 processes acting on the water vapor mainly derived from deep convection. These thin tropopause
239 layer clouds can be formed in situ due to adiabatic ascent associated with equatorial waves such
240 as the Kelvin wave [Boehm and Verlinde, 2000]. In the few kilometers at and just below the
241 tropopause, laminar, optically thin (often subvisible) cirrus occur frequently.

242 Thin cirrus in the TTL occurs with very high frequency and likely plays a central role in
243 regulating the water vapor concentration of the stratosphere. TTL cirrus has been observed with
244 a number of satellites, including SAGE II, HALOE, and HIRDLS. More recently, CALIPSO
245 measurements are providing a wealth of information about optically thin TTL cirrus regional
246 distribution, structure, and extinction. In situ observations of TTL cirrus are limited, primarily
247 because high altitude aircraft are required to sample them.

248 An understanding of the detailed processes of TTL cirrus formation is necessary for
249 quantitative prediction of their impact on the water vapor and radiation budgets. Recent in situ
250 observations suggest large supersaturations can occur both within TTL cirrus and in clear regions
251 near the cold tropical tropopause (Gao *et al.* [2004], Jensen *et al.*, [2005]). The existence of such
252 large supersaturations (relative humidities with respect to ice (RHI) sometimes approaching
253 200%) defies theoretical expectations that ice crystals will nucleate at 160% RHI, preventing
254 further increase in supersaturation, and that within TTL cirrus, ice crystal growth should rapidly
255 deplete vapor in excess of saturation. However, these high-supersaturation measurements have
256 been called into question because of persistent discrepancies in water vapor measurements made
257 by different instruments [Jensen *et al.*, 2005; Kramer *et al.*, 2009].

258 In addition to the issues involving large supersaturations at low temperatures, there are
259 significant gaps in our understanding of how cirrus forms at very low temperatures. The
260 conventional theory is that homogeneous freezing of aqueous aerosols dominates production of
261 ice crystals in the upper troposphere. However, recent measurements of TTL cirrus ice
262 concentrations, particle size distributions, and cloud extinctions are in conflict with theoretical
263 expectations for cirrus formed via homogeneous freezing at low temperatures [Jensen *et al.*,
264 2008].

265

266 **2.4 The TTL thermal budget**

267

268 As discussed above, under clear-sky conditions, the upper part of the TTL is radiatively
269 heated. In balance with this heating, the air is slowly ascending into the stratosphere. The rate of
270 vertical transport through the TTL and lower stratosphere has been estimated from observations
271 of the water vapor “tape recorder” [Mote *et al.*, 1996; Niwano *et al.*, 2003; Schoeberl *et al.*,
272 2008], from observations of the CO₂ gradient in the TTL [Park *et al.*, 2007], and from radiative
273 transfer calculations [Rosenlof *et al.*, 1997]. It has also been pointed out that the TTL radiative

274 heating rate depends on the presence of lower clouds; when cold, optically thick anvil cirrus is
275 present below the TTL, the TTL will experience radiative cooling [*Hartmann et al.*, 2001].

276 Recently, it has been recognized that cirrus within the TTL play an important role in the
277 thermal budget. Radiative transfer calculations have shown that thin cirrus in the TTL can
278 experience radiative heating of a few K/day [*Jensen et al.*, 1996; *McFarquhar et al.*, 2000;
279 *Comstock et al.*, 2002]. *Corti et al.* [2006] suggested that radiative heating in TTL cirrus
280 accounts for a large fraction of the total radiative heating in the TTL, and that radiatively-driven
281 lofting of cirrus may account for much the vertical transport from the main convective outflow
282 level below the TTL up to the tropopause (see Figure 2). Measurements of TTL cirrus radiative
283 heating rates, along with the microphysical properties of the clouds would be very useful for
284 constraining radiative transfer calculations of TTL cirrus impacts on TTL heating and vertical
285 transport.

286 The ultimate role of tropical cirrus in future climate change involves feedback effects. For
287 example, anthropogenic greenhouse gases can increase the surface temperature, possibly
288 resulting in increased frequency and intensity of convective storms. Increased convection
289 intensity could alter tropical cirrus cloudiness, with corresponding effects on the Earth radiation
290 budget and additional surface temperature changes. Hence, the net effect of increased greenhouse
291 gas concentrations on surface temperature depends on the response of convection and cirrus to
292 the changing environment. Prediction of these feedback effects requires understanding of the
293 full cirrus lifecycle from generation in deep convection to horizontal spreading and ultimate
294 dissipation. Understanding the balance between remote and local dynamical response to
295 intensifying deep convection is a key issue, i.e. whether the local induced subsidence field is
296 enhanced with resulting less or shorter-lived cirrus. Tropical cirrus may also be changing in
297 response to anthropogenic aerosols. Particles from industrial activity or biomass burning may
298 affect ice nucleation in the convective updrafts, ultimately changing the numbers and sizes of
299 cirrus ice crystals. Likewise particulate and gaseous emissions that produce particulates, from
300 either aircraft or volcanic eruptions, could alter cirrus properties. These cirrus modifications
301 would ultimately affect radiation budgets and climate. While we know little about the
302 composition or origins of aerosols in the tropical upper troposphere, recent work suggests that
303 tropical cirrus that can be traced to deep convection do show a sensitivity to their convective
304 sources. *Mace et al.* [2005] show results suggesting that cirrus that originate from convection
305 near major islands in the western Pacific tend to be composed of higher numbers of small
306 particles compared to cirrus that originate in purely maritime convection. Recent field programs
307 have shown surprisingly large amounts of organics, as well as metal and carbonaceous particles
308 in the upper troposphere.

309 310 **2.5. The chemical fates of short-lived compounds transported from the tropical boundary** 311 **layer into the TTL** 312

313 Until recently, the chemical precursors of the stratospheric radicals and aerosol, with the
314 notable exception of water vapor, were thought to be compounds with long tropospheric
315 lifetimes. This greatly simplified defining the chemical boundary condition for the stratosphere
316 because globally-averaged surface measurements of these long-lived compounds could be used.
317 For example, sulfur was thought to be carried mainly by carbonyl sulfide, nitrogen by N₂O, and
318 halogens by the relatively long-lived halocarbons.

319 It has become increasingly clear, however, that short-lived compounds transported to the
320 tropopause region of the tropics significantly alter the chemistry of the global stratosphere. The
321 amount of OCS transported across the tropopause accounts for no more than half of the sulfur
322 aerosol present in the lower and middle stratosphere [e.g., Weisenstein et al., 1997]. The
323 remainder may come from small volcanic eruptions venting into the lower stratosphere, or from
324 tropospheric sulfate and sulfur gases that are transported across the tropical tropopause. Thus,
325 our understanding of how the “background” sulfate aerosol layer is maintained is incomplete.
326 Bromine monoxide concentrations in the lower stratosphere appear to reflect the input of very
327 short-lived bromine containing organic, and perhaps inorganic, compounds [e.g., Ko et al., 1997;
328 Pfeilsticker et al., 2000], possibly leading to a much larger role for catalytic loss of lower
329 stratospheric ozone by halogens than is considered in most models [Dvortsov et al., 1999].
330 Finally, the concentration of reactive nitrogen, NO_y , and ozone are non-zero at the tropical
331 tropopause [Strahan, 1999]. Release of NO_x from NO_y carried across the tropopause will likely
332 have important implications for the efficiency of ozone loss by halogen cycles in the lower
333 stratosphere. The NO_y/O_3 ratio can provide an important test of the realism of transport models
334 for both the lower stratosphere and upper troposphere provided the sources of both species are
335 understood [e.g., Murphy et al., 1993].

336 Observations of short-lived sulfur, nitrogen, and halogen-containing compounds in the
337 region of the tropical tropopause are sparse. Acquiring such measurements is essential to
338 accurately assess the effect on ozone of future changes in halogen loading, stratospheric sulfate
339 aerosol abundance, and changes in tropical convection that might be associated with climate
340 change. Estimates of the ozone depletion potential of short-lived halogen species depend on a
341 quantitative evaluation of the efficiency of transport from source regions into the TTL and
342 subsequent transport across the tropical tropopause. An understanding of the relative roles of
343 (slow) large-scale transport and rapid convective transport and a better understanding of the
344 chemistry of short-lived species in the UT and TTL is crucial to the improvement of such
345 estimates [Ko and Poulet, 2002]. The observations of short-lived species in TC4 will address
346 these issues and will provide new understanding of dynamics in the UT and TTL regions. The
347 interesting species for measurement have a range of photochemical lifetimes (e.g., 0.003 days for
348 CH_2I_2 ; 4 to 7 days for CH_3I ; 36 days for CHBr_3), and thus can be used to diagnose transport
349 characteristics of the TTL on a variety of spatial and temporal scales.

350

351 **2.6. The mechanisms that control ozone below and within the TTL**

352

353 Ozone concentrations in the TTL are determined by a complicated interplay of convective
354 processes (that transport both ozone and short-lived compounds that fuel further ozone
355 production from the lower troposphere), in situ photochemistry, and large-scale dynamics.
356 Diagnosing this diversity of processes – occurring over large spatial and time scales – provides a
357 challenging, but important, observational problem. To date, very few observations are available
358 to test our understanding of the mechanisms that control ozone in the TTL.

359 Photochemistry within the TTL is thought to lead to significant in situ ozone production.
360 This production results primarily from the oxidation of CO by OH in the presence of nitrogen
361 oxides. Ozone formation due to photolysis of molecular oxygen can also be important, because
362 the stratospheric ozone column is relatively low in the tropics. Since the chemical lifetime of
363 ozone with respect to photochemical loss is long (several months), the TTL is a region of
364 significant net production for tropospheric ozone.

365 Our current understanding of tropical tropospheric ozone in general is based primarily on
366 insights drawn from analyses of data from aircraft campaigns and ozonesondes, and on model
367 studies. In the upper tropical troposphere ($z > 12$ km), analysis of the few profiles obtained by the
368 NASA ER-2, have demonstrated that HO_x photochemistry and its impact on ozone in this region
369 is poorly understood [McKee *et al.*, 1997, Folkins *et al.*, 1997, Jaeglé *et al.*, 1997, Wennberg *et*
370 *al.*, 1998]. HO_x concentrations are much larger than expected based on H₂O/O₃ photochemistry.
371 The high levels of HO_x observed, along with high NO_x, possibly associated with biomass
372 burning, suggest elevated ozone production. Below 12 km, (restricted by the flight altitude of
373 the DC-8), major campaigns have taken place in the south tropical Atlantic (TRACE-A), or in
374 the Pacific, flying out of Hawaii, Fiji, and Tahiti (PEM-Tropics A and B). Analyses of data from
375 these campaigns have shown the importance of ozone precursor emissions from biomass burning
376 in the dry season, and have also invoked an important role for lightning as source of NO_x upwind
377 of the region of the measurements [Thompson *et al.*, 1996; Jenkins *et al.* 1997; Schultz *et al.*,
378 1999; Staudt *et al.*, 2002, 2003]. Over both the Pacific and South Atlantic photochemical
379 reactions, provide a net source for ozone above about 7 km and a net sink below, a consequence
380 of the rapid decrease in water vapor with height. Over the tropical Pacific, production balances
381 only about half of the column ozone loss below 12 km, indicating that there is significant
382 transport of ozone to the Pacific [e.g., Schultz *et al.*, 1999; Wang *et al.*, 2001].

383 As is clear from the above discussion, convection plays a key role in influencing the
384 distribution of tropical ozone, both in terms of mixing ozone and its precursors out of the
385 boundary layer over continental source regions (e.g., regions of biomass burning), and in mixing
386 extremely low ozone values from either the marine boundary layer over the Pacific or unpolluted
387 continental areas into the upper troposphere, as shown by analyses of ozonesonde data [Kley *et*
388 *al.*, 1996; Oltmans *et al.*, 2001]. Lightning associated with convective systems will also provide
389 a source of NO_x, enhancing photochemical ozone production.

390 Analyses of ozone sonde profiles from Samoa have shown that ozone mixing ratios usually
391 start to increase in the TTL around 14 km, well below the tropical tropopause [Folkins *et al.*
392 1999], although the largest change in gradient in the ozone mixing ratio is near the thermal
393 tropopause. Folkins *et al.* [1999] argue that the increase in ozone is caused by the suppression of
394 vertical mixing associated with convection above 14 km, and that the positive correlation they
395 find between potential temperature and ozone above 14 km is consistent with slow large scale
396 ascent, positive radiative heating, and photochemical production of ozone. They also argue that
397 some of the ozone originates from the stratosphere, based on correlations with N₂O.

398 Increases in ozone well below the thermal tropopause are found at tropical ozonesonde sites
399 in the Pacific, the Atlantic, and Africa. (The thermal tropopause is the World Meteorological
400 Organization defined tropopause based on the lapse rate, which is generally lower in altitude
401 than the cold point tropopause). Inspection of individual profiles shows that this is not always
402 the case, particularly in the western Pacific (Logan, unpublished work). The significant
403 longitudinal gradients in tropical ozone, with values over the Atlantic higher than those over the
404 Pacific year-round, extend all the way to the thermal tropopause [Logan, 1999; Thompson *et al.*,
405 2003a].

406 Long-lived tracers in TC4 should provide the foundation for diagnosing the processes that
407 are responsible for atmospheric transport on the largest time and space scales (Figure 2). They
408 should also provide a bridge tying together the objectives for the mission in mid-tropospheric
409 chemistry, input processes to the stratosphere in the TTL, black carbon sources and distributions,
410 and convective cloudiness and transport of water vapor.

411 The land has very large exchange fluxes of CO₂ between the surface and the atmosphere.
412 The signals from these fluxes appear above the stable marine planetary boundary layer (PBL),
413 maintaining distinctive gradients between the marine PBL and the mid-troposphere such as
414 observed in CRYSTAL-FACE, providing a unique tracer for convective redistribution. The
415 seasonal cycle of CO₂ also offers an excellent age-of-air tracer for the TTL.

416 Concentrations of SF₆ and/or HCFCs are growing rapidly in the atmosphere due to
417 industrial sources predominantly in the northern hemisphere. These gases display distinctive
418 North/South gradients and thus provide good indicators of the hemisphere of origin for air in the
419 study domain. They also represent independent age-of-air tracers, albeit usually less sensitive
420 than the CO₂ seasonal cycle.

421

422 **2.7. Linking satellite and aircraft data**

423

424 Resolution of many of the issues discussed above will require remote sensing measurements
425 from satellite instruments with near global spatial coverage and multi-year temporal coverage.
426 For example, understanding how cirrus clouds impact regional and global upper tropospheric
427 humidity clearly requires analysis of large-scale fields of cloudiness and H₂O abundance.
428 Remote sensing constituted an important part of the TC4 measurement campaign by providing
429 the horizontal distributions of cloud properties and gas concentrations at a variety of spatial and
430 temporal scales. Cirrus cloud properties also vary on small spatial scales, and in situ
431 observations of ice crystal size distributions, total condensed water, and extinction will be critical
432 for validating algorithms applied to remote sensing measurements.

433 There are numerous examples of field programs involving aircraft and balloon platforms
434 that have successfully linked with satellite validation ranging back over at least two decades.
435 The SOLVE-2 program was aimed at validating SAGE III, which obtains profiles of aerosols,
436 ozone, and a number of other chemical species at high latitudes. Measurements obtained during
437 SOLVE-1/THESEO-2000 provided validation of chemical ozone loss rates, O₃ and H₂O profiles,
438 and polar stratospheric cloud detection and analyses (e.g., denitrification inferred from PSC
439 formation temperature) from the Naval Research Laboratory Polar Ozone and Aerosol Monitor
440 (POAM) III satellite instrument [Newman et al., 2002]. Aircraft measurements of CO from the
441 DC-8 during TRACE-P provided validation of MOPITT data on Terra [Jacob et al., 2003].
442 Satellite remote sensing was a central theme of CRYSTAL-FACE [Jensen et al., 2004].
443 CRYSTAL-FACE provided validation opportunities for Terra, Aqua and TRMM. Not only were
444 cloud property retrieval algorithms tested, but specific case studies were proposed by the satellite
445 groups and carried out. Some of these involved clear sky data as well as cloudy data. The TC4
446 field campaign supported validation efforts of the entire “A train” –Aura, CALIPSO, CloudSat,
447 PARASOL and Aqua. It also provided validation opportunities for Terra and TRMM.

448 The Aura satellite, a principal focus of TC4, provides essential information on the spatial
449 and temporal variability of key constituents in the TTL region (such as ozone, water vapor, CO,
450 and thin cirrus clouds) with horizontal and vertical resolutions not previously available from
451 satellite observations. Satellite observations in this region are, however, generally more
452 challenging than measurements at higher altitudes due to the cloud cover.

453

454 **3. Mission scope**

455

456 The NASA Earth Science Project Office (ESPO) began preparations for TC4 in September
457 2006. Site visits to Panama and Costa Rica were first made to determine the ideal location to
458 base the mission. San Jose, Costa Rica was chosen as the primary site for the aircraft and most
459 personnel based on local weather and existing infrastructure. Meetings with the U.S. Embassy
460 personnel, Ministers of Transportation and Science, National Science Center, Director of General
461 Civil Aviation, and Airport Management to work out all the mission details were critical to the
462 unique operation of TC-4.

463 A large amount of work was performed on the hangars, lab / office modifications, and
464 obtaining all the lab and aircraft ground support equipment required for the mission. In addition,
465 ESPO setup all the communications, housing, security badging, medical services, and local
466 transportation that would be needed for the hundreds of people who would travel to Costa Rica
467 during the six-week deployment. International agreements for the aircraft overflight and
468 personnel country clearances were also arranged with all the various countries.

469 Over 70 instruments were integrated onto the 3 aircraft based at different locations. The DC-
470 8 was integrated at McClellan Field in California, the ER-2 at NASA's Dryden Flight Research
471 Center in California, and the WB-57F at NASA's Ellington Field in Houston, Texas. ESPO
472 made appropriate arrangements for access, equipment and integration support for the aircraft
473 teams. ESPO provided coordination and support at each of these integration sites and managed
474 the C-5 military airlifts to transport all the aircraft and investigator equipment to and from the
475 mission deployment site.

476 In Las Tablas, Panama, preparations were made for the NPOL radar and NATIVE
477 atmospheric research trailer. The ground site required a road to be built, the hill leveled, and
478 electricity to be brought to the site. Because of the remoteness of the site, communications were
479 obtained through a portable KU satellite ground station provided by NASA Ames Research
480 Center.

481 The Embassies, local governments and universities all provided valuable support. The
482 cooperation and support from the Costa Rican and Panamanian officials, professionals and
483 scientists were both appreciated and absolutely essential for TC4's success.

484

485 **3.1 Location and timing**

486

487 The TC4 aircraft were based at the Juan Santamaria International Airport in Alajuela, a
488 suburb of San Jose, Costa Rica (10.0°N, 84.22°W) (Figure 1). The first data flights were made
489 on 17 July, 2007 and the last data flight from Costa Rica was made on 8 August, 2007 (Table 2).
490 The WB57-f made one additional data flight from Houston, Texas on 13 August, 2007. The
491 final date of the field mission was chosen to minimize the chance of tropical storms or
492 hurricanes, which become more likely in September. The initial dates of the field mission were
493 chosen to maximize the chance that the intertropical convergence zone (ITCZ) with its extensive
494 convective activity, would be near Costa Rica.

495 The President of Costa Rica, Noble Peace Prize winner Oscar Arias Sanchez, generously
496 lent us the hangar normally used for his own aircraft to house the ER-2. The WB-57F used a
497 clam-shell hangar that was built by NASA and Costa Rica for research programs such as TC4.
498 The DC-8 was stationed on the ramp used by commercial aircraft.

499 In addition to the aircraft, balloons and a Doppler radar (the Shared Mobile Atmospheric
500 Research and Teaching Radar, SMART-R) were positioned at the Juan Santamaria airport.

501 A polarization radar (NPOL), a ground station (NATIVE), and further balloon launches
502 were conducted from Las Tablas, Panama. This location was chosen because of its proximity to
503 the Gulf of Panama. It was expected that convection would form frequently in the Gulf and that
504 the aircraft would be able to fly into the anvils of these clouds guided by the radar. While such
505 flights did occur, the convection over the Gulf of Panama was often very intense, and low wind
506 shear kept the anvils near the convective updrafts. These conditions made it difficult to safely
507 operate the aircraft over the Gulf of Panama.

508 Balloon launches were also conducted from San Cristobal a SHADOZ site [Thompson *et al.*,
509 2003b] in the Galapagos Islands. This has been a water vapor measurement site since 1998
510 (Vömel *et al.*, 2002).

511

512 **3.2 Platforms**

513 Here we discuss the numerous platforms used in TC4 including satellites, aircraft, balloons
514 and ground based facilities.

515

516 **3.2.1 Satellites**

517

518 A number of satellites were employed as discussed below.

519

520 **3.2.1.1 Aura**

521

522 AURA has four instruments designed to measure air chemistry (Table 3). Operational
523 considerations required that the ER-2 and WB-57F land before the mid-afternoon over-flight
524 times of AURA. However, the DC-8 was able to make a large number of flights under various
525 Aura instruments. Since the AURA instruments have variable fields of view, it generally was
526 only possible to be directly in the field of view of a single instrument during the satellite
527 overpass.

528 Many of the DC-8 flights were aimed at the OMI instrument, and determining if SO₂
529 emissions from South American volcanoes were properly evaluated.

530

531 **3.2.1.2. MODIS**

532

533 The MODIS instruments on the Terra and Aqua satellites routinely retrieve cloud properties
534 from all types of tropospheric clouds. Because of the wide observing area, it was often possible
535 to underfly the Terra satellite during its morning overpass. Hence the TC4 aircraft were able to
536 investigate such retrieved parameters as cloud top and base heights, cloud particle size and cloud
537 ice water content. The DC-8 was also able to underfly Aqua along with the rest of the A-Train
538 satellites.

539

540 **3.2.1.3 CloudSat and CALIPSO**

541

542 CloudSat and CALIPSO, along with Aura, are part of the A-Train constellation of satellites
543 which all pass a given spot on Earth within a few minutes of each other. CloudSat obtains radar
544 backscatter data, while the CALIOP instrument on CALIPSO uses a lidar to sense optically thin
545 clouds. Numerous DC-8 flights had segments dedicated to underflying these instruments. For
546 instance, flights were made to investigate the properties of marine boundary layer clouds to help

547 interpret the satellite observations near the surface. The ER-2 radars also profiled a number of
548 cloud systems for comparison with the data from these satellites.

549

550 **3.2.1.4 TRMM**

551

552 The instruments on the TRMM satellite are aimed at measuring precipitation. Underflights
553 for comparison with the ER-2 and DC-8 radars were made.

554

555 **3.2.2. Aircraft**

556

557 Three NASA aircraft were employed in TC4.

558

559 **3.2.2.1 ER-2**

560

561 The NASA ER-2 is the civilian version of the second generation Lockheed U-2 high-
562 altitude aircraft. The ER-2 has flown in numerous field campaigns. It is capable of flights above
563 20 km (pressures less than 50 hPa) for durations up to 8 hours. The ER-2 flew 13 science flights
564 in TC4 including the transit flights (Table 2).

565 The ER-2 aircraft was used as a remote sensing platform. Its basic goal was to simulate
566 various satellite instruments so that more prolonged comparisons of in situ and remote sensing
567 data could be made than would be possible between satellites and aircraft. Figure 3 illustrates
568 the ER-2 with the locations of the 11 instruments. Table 4 lists the ER-2 instruments, their PI,
569 and provides a brief summary of their measurement capabilities. Video from the ER-2 camera is
570 available at <ftp://asapdata.arc.nasa.gov/outgoing/MVIS/TC4/>.

571

572 **3.2.2.2 WB-57F**

573

574 The NASA WB-57F has been flying research missions since the 1960s when it was
575 originally used for sampling the atmosphere for the debris from nuclear weapons tests. The
576 aircraft is capable of flights to 60,000 ft (19.4 km) for durations approaching 6.5 hours. Prior to
577 the start of TC4 the WB-57F suffered a fire in its landing gear which damaged panels on the
578 wing. It was, therefore, delayed in arriving in Costa Rica. The WB-57F flew 6 science flights in
579 TC4 including 2 ferry flights, and one local science flight from Huston, Texas.

580 The WB-57F was used as an in situ sampling aircraft in TC4. One of its major goals was to
581 underfly the ER-2 and measure cloud properties as seen by the ER-2 remote sensing instrument.
582 It was also well instrumented with in situ instruments for sampling tracers of air motion, and
583 trace gases. Figure 4 illustrates the WB-57F with the locations of the 25 instruments. Tables
584 5a,5b list the WB-57F instruments, their PI, and provides a brief summary of their measurement
585 capabilities.

586

587 **3.2.2.3 DC-8**

588

589 The NASA DC-8, managed during TC4 by the University of North Dakota, is a former
590 commercial airliner that has been converted into a flying laboratory. The DC-8 has been
591 deployed in numerous field campaigns. The aircraft is capable of flights to an altitude of 12 km
592 for durations over 10 hours. It made 13 science flights during TC4 including the transit flights

593 (Table 2).

594

595 The DC-8 was used in TC4 both to remotely sample the atmosphere and to make in situ
596 measurements of aerosols, clouds and gases. While numerous flight segments were flown in
597 anvils, a number of flight segments were also flown to investigate emissions from volcanoes and
598 from the jungles of Central and South America. The aircraft is shown in Figure 5, with the
599 locations of the 25 instruments. The DC-8 instruments are listed in Table 6 along with the PI,
600 and an overview of the measurements.

601

602 **3.2.3 Balloonsondes**

603

604 Several balloon programs were included in TC4.

605

606 **3.2.3.1 Ticosonde**

607

608 A total of 214 Vaisala RS92-SGP radiosondes were released at Juan Santamaria
609 International Airport between 16 June and 15 August by the Ticosonde-TC4 project. Launches
610 were made twice daily at 00 and 12 UT through 30 June and four times daily at 00, 06, 12 and 18
611 UT thereafter. As outlined in Table 7 the sondes provided pressure, temperature, relative
612 humidity and GPS winds every two seconds up to a campaign-average altitude of 30.1 km.

613 The Ticosonde-TC4 project was led by Dr. Henry Selkirk of the BAER Institute of Sonoma,
614 California and NASA-Ames Research Center, in collaboration with Profs. Walter Fernandez and
615 Jorge Andrés Diaz of the Escuela de Fisica at the Universidad de Costa Rica (UCR), Prof. Jorge
616 Amador of the Centro de Investigaciones Fisicas at UCR, Werner Stolz of the Instituto
617 Meteorologico Nacional (IMN) and Dr. Pedro León of the Centro Nacional de Alta Tecnologia
618 (CeNAT). Launches were conducted by IMN personnel in collaboration with UCR students at
619 the IMN sonde site at the west end of the airport.

620

621 **3.2.3.2 CFH-ozonesonde launch programs**

622

623 A team led by Dr. Holger Vömel of the University of Colorado (CU) and the NOAA Earth
624 Systems Research Laboratory (ESRL) (now at Deutscher Wetterdienst, Meteorological
625 Observatory Lindenberg) made 15 launches of balloons carrying the CU Cryogenic Frostpoint
626 Hygrometer (CFH) [Vömel, *et al.*, 2007a] and the ECC ozonesonde [Komhyr, *et al.*, 1995] from
627 the IMN sonde site. The CFH-ozonesonde launch program was a partnership with IMN and Dr.
628 Jessica Valverde of the Universidad Nacional (UNA) and IMN. The CFH/ozonesonde launches
629 were made approximately every other day during the aircraft flight campaign by a team
630 composed of IMN staff and students from UNA. The typical altitude achieved by the 1200-g CU
631 balloons was 30 km. Dr. Vömel also cooperated with the Instituto Nacional de Meteorología y
632 Hidrología de Ecuador to conduct a simultaneous CFH/ozone sonde launch program at San
633 Cristobal, Galapagos.

634 A team led by Dr. Sergei Khaykin of the Central Aerological Observatory in Dolgoprudny,
635 Russia flew their Lyman- α FLASH-B (FLuorescent Advanced Stratospheric Hygrometer)
636 hygrometer [Vömel, *et al.*, 2007b] along with the CFH on 5 nighttime ascents.

637

638

639 **3.2.3.3 NATIVE balloons**

640

641 Launches of both radiosondes and the water vapor- and ozonesondes were coordinated with
642 ozonesonde launches at Las Tablas, Panama, by a team led by Profs. Anne M. Thompson of the
643 Penn State University and Gary Morris of Valparaiso University.

644

645 **3.2.4 Radars**

646

647 Two radars were used in TC4.

648

649 **3.2.4.1 SMART**

650

651 Dr. Michael Biggerstaff from the University of Oklahoma led the first international
652 deployment of the Shared Mobile Atmospheric Research and Teaching Radar (SMART-R)
653 during the NASA TC4 experiment. The radar was located near the west end of the Juan
654 Santamaria International Airport in Costa Rica (Figure 6), where it was used to provide real-time
655 flight support for NASA's DC-8, ER-2, and WB-57 aircraft. The SMART radar was the first
656 Doppler radar to ever have been deployed in Costa Rica and provided insight into the structure
657 and timing of the modified land-sea breeze circulation that initiates afternoon thunderstorms over
658 the airport on a regular basis.

659

660 **3.2.4.2 NPOL**

661

662 The NASA Polarimetric (NPOL) research radar is a state-of-the-art weather research radar.
663 It was based near the Gulf of Panama at Las Tablas, Panama (see Fig. 7). The goal of this radar
664 was to observe deep convective systems developing in the Gulf of Panama, and to safely guide
665 research aircraft into the anvils of cumulus.

666

667 **3.2.5 Ground based stations**

668

669 The Nittany Atmospheric Trailer and Integrated Validation Experiment (NATIVE) is a self-
670 contained, state of the art, mobile research facility designed for satellite validation, air quality
671 monitoring, investigations of pollution transport and deposition, and for use as an educational
672 outreach tool (see Fig. 7). The facility houses a suite of in situ trace as instruments, active and
673 passive remote sensing instruments for atmospheric profile and column measurements, and
674 several meteorological probes. The satellite communication system allows NATIVE to
675 disseminate results in near real time.

676

677 **4. Mission forecasting and aircraft coordination**

678

679 While forecasts were important in setting up the flight profiles, in practice the aircraft were
680 guided to interesting phenomena in real time. We describe both of these activities below.

681

682 **4.1 Forecasting**

683

684 Mission forecasting was led by Drs. Lenny Pfister and Henry Selkirk in conjunction with
local forecasters from Costa Rica. Two aspects of the mission depended on the forecasting

685 group. Daily forecasts were used to determine the locations of promising meteorological targets,
686 such as convection, and to determine if adverse weather might prevent safe mission operations.
687 Fortunately no tropical storms occurred during TC4, and no missions were cancelled due to
688 weather. However, intense afternoon convection at the Juan Santamaria was almost a daily
689 occurrence. On several occasions commercial airliners had to be diverted, experienced long
690 weather delays, or landed in heavy rainfall with lightning in the area. None of these conditions
691 were desirable for landing, particularly for the ER-2 and WB-57F. Aside from aircraft safety,
692 heavy rain could damage instruments before the aircraft could be put into their hangars.

693 As a consequence of the severe afternoon weather we relied heavily on the Costa Rican
694 forecasters to predict the time of onset of convection. Generally, we planned to land the ER-2
695 and WB-57F between noon and 2pm, to avoid convection. We also monitored the local
696 convection while the aircraft were in flight. The skill of the forecasters was a critical element in
697 not having to divert any aircraft, and in generally being able to hangar the aircraft before tropical
698 downpours began.

699
700

701 **4.2 Real time flight plan coordination**

702 There are a number of reasons to control research aircraft in real time. When sampling the
703 anvils of mesoscale convective complexes, safety requires that the aircraft stay away from the
704 convective cores, or at least sample cores that have weak updrafts, or are decaying. In addition,
705 given real time knowledge of the locations of interesting atmospheric phenomena, nearly
706 instantaneous aircraft control allows one to change opportunistic sampling into controlled
707 investigations. During the CRYSTAL-FACE mission in July 2002 in Southern Florida, we were
708 able to use the large number of Doppler radars in Florida together with the U.S. air traffic control
709 reporting information, which is based on aircraft transponders, to navigate as many as 5 aircraft
710 in real time. In contrast, Costa Rica has no weather radars, even at its main airport, and does not
711 provide tracking information on aircraft.

712 NASA installed Research Environment for Vehicle Embedded Analysis on Linux
713 (REVEAL) systems on a number of aircraft including the DC-8, ER-2 and WB-57F. TC4 was
714 the first opportunity to employ REVEAL on all of these aircraft simultaneously. REVEAL ,
715 developed and supported NASA Dryden Flight Research Center, allows aircraft location, and
716 instrument data to be reported back to mission operations. It also allows for scientists on the
717 ground to communicate back to the NASA DC-8 flight scientist to discuss changes in flight
718 plans. In conjunction with REVEAL, the Real Time Mission Monitor (RTMM), developed and
719 supported by the NASA Marshall Space Flight Center, allowed us to locate the aircraft on a
720 virtual Earth display, track their motions in the context of meteorological data, and to down-link
721 data from the aircraft that could be used to alter the aircraft flight plans in real time. For
722 example, the mission operations group was able to see in near real time the aircraft locations,
723 several satellite data sets on clouds, data on recent lightning strikes, and data from our own
724 aircraft including lidar profiles of clouds. Using tools developed by Dr. Pat Minnis and his
725 group at NASA Langley we were also able to combine the aircraft location data with GOES
726 Rapid Scan data to aid in detecting fresh convective cells embedded in the mesoscale clusters we
727 were studying. Finally, we had real time data from the NPOL and SMART radars to help locate
728 the aircraft relative to convection in flights near the Gulf of Panama, or on return to the Juan
729 Santamaria airport in Costa Rica.

730 As discussed below, many of our flight plans involved coordinated flights for several
731 aircraft early in a mission, and then different flight plans at the end of the mission. These flight
732 plans were partly the result of the short flight duration of the WB-57F relative to the other
733 aircraft. However, they also reflected the strong diurnal cycle of convection at the Juan
734 Santamaria airport. Generally the ER-2 and WB-57 had landing times in the period from noon to
735 2pm local to avoid bad weather on landing. However, the DC-8 is less sensitive to weather
736 conditions on landing than the other aircraft. The DC-8 often returned in the late afternoon,
737 commonly in heavy rainfall.

738 Animated overlays of the flight tracks and various satellite observed and derived cloud
739 parameters can be found at <http://www-angler.larc.nasa.gov/TC4/fltrks>. Animated overlays of
740 observed quantities including lightning strikes can be found at
741 <http://rtmm.nsstc.nasa.gov/movies-TC4.html>. Examples will be discussed below.

742

743 **5. Aircraft Flights**

744

745 Table 2 outlines the aircraft flights made during TC4. Flight plans and flight reports are
746 available at <http://www.espo.nasa.gov/TC4/flightDocs.php>. We will discuss the flights
747 individually below.

748

749 **5.1. 17 July, 2007**

750

751 Figure 8 illustrates the flight tracks for the ER-2 and DC-8 on 17 July, 2007. The aircraft
752 linked up south of a large mesoscale complex off the Pacific coast of Costa Rica. The aircraft
753 then did several oval loops, or racetracks, with the DC-8 sampling cirrus anvils from the cloud
754 system, and the ER-2 remotely observing the cloud field from above. The ER-2 then returned to
755 San Jose flying over the cores of several convective cells during a TRMM overpass. The DC-8
756 flew along the coast of Ecuador to sample the emissions from volcanoes, and then flew along a
757 HIRDLS track for the Aura satellite before returning to Costa Rica. In Figure 8 the flight tracks
758 are superimposed on cloud optical depths retrieved from the GOES satellite data. Note that the
759 three racetracks flown by the aircraft are in low optical depth cirrus rather than in the high
760 optical depth portion of the cloud north of the racetrack. The region to the South of the image is
761 black, because that marks the southern boundary of the GOES 12 observations.

762

763 **5.2 July 19, 2007**

764

765 Figure 9 illustrates the flight track for the ER-2 on 19 July, 2007. The DC-8 did not fly due
766 to a mechanical problem. The ER-2 first flew over the Pacific to profile the cores of several
767 convective systems. It then flew over the Caribbean where it detected low-lying layers of
768 Saharan dust, whose presence had been predicted. The aircraft also observed a high altitude,
769 optically thin cirrus cloud as it returned to Costa Rica.

770

771 **5.3 21 July, 2007**

772 Figure 10 illustrates the DC-8 flight track on 21 July, 2007 superimposed on a GOES 10+12
773 composite visible image. The ER-2 had a mechanical problem on this day and did not fly. The
774 flight began with a low-level run to sample the marine boundary layer over the Pacific, and then
775 sampled cirrus in the convective regions over the Gulf of Panama. The DC-8 then proceeded to

776 Colombia to sample the plume of the volcano Nevado de Huila, which shows up on OMI SO₂
777 imagery. The DC-8 then turned north to obtain a trace-gas sample of the Colombian farming
778 regions, which may be a source of methane. Finally the DC-8 sampled Saharan dust aerosols in
779 the Caribbean, of the sort sampled by the ER-2 on 19 July, and returned to Costa Rica.
780

781 **5.4 22 July, 2007**

782 Shortly after takeoff, the DC-8 headed southwest into the Pacific and descended into the
783 boundary layer for aerosols and chemistry sampling as shown in Figure 11. An ITCZ convective
784 system was sampled, and a box pattern was set up for sampling the outflow cirrus. The long
785 sides of the rectangle were oriented approximately across the mean wind direction. This strategy
786 allowed the DC-8 to sample many distinct outflows from individual convective cells, with the
787 ER-2 directly overhead. The DC-8 vertically profiled several times through the outflow cirrus (in
788 and out of cloud) between about 7.6 and 10.6 km in close coordination with the ER-2. When the
789 outflow cirrus appeared to be dissipating, the DC-8 did several penetrations through small,
790 developing convective turrets at temperatures ranging from 200 to 255 K before heading west to
791 Panama to sample cirrus generated by Gulf of Panama convection earlier in the day. The along-
792 wind track took the DC-8 through two separate anvil outflows that were streaming
793 southwestward from dissipating convective sources. The DC-8 did two legs, coordinated with
794 ER-2 profiling enroute through the cirrus between about 7.6 and 11.6 km. Crystals as large as 3
795 mm and ice water contents as large as 0.3 g/m³ were detected over the Gulf of Panama. The ER-
796 2 departed for Costa Rica, while the DC-8 headed north along the CloudSat/CALIPSO track,
797 flying through optically thin cirrus at about 12 to 12.5 km which existed above a mostly cloud
798 free ocean surface. This cirrus contained pristine ice crystals (bullet rosettes were noted on the
799 CPI). CloudSat and CALIPSO passed overhead as the DC-8 approached its most northerly point
800 on the several-hundred-km leg. At that point, the DC-8 turned back south along the satellite track
801 and, after an Air Traffic Control delay, spiraled down into the boundary layer to sample Saharan
802 dust below 4 km indicated by the DC-8 lidars. After stepping up to about 2 and 3 km, the DC-8
803 returned to base. Over the entire flight profiles of aerosols, tracers, and chemical species were
804 collected from the boundary layer to the upper troposphere both in the Pacific and Caribbean,
805 and a variety of types of anvil outflow cirrus were sampled in situ.
806

807 **5.5 24 July, 2007**

808
809 As shown in Figure 12, the DC-8 first did a low-level run through the boundary layer
810 around a convective system. It then ascended to near 20,000 feet where the plane was struck by
811 lightning twice in a rapidly developing system. The DC-8 then did the boundary layer run again
812 and ascended to 36 kft to probe the cirrus layer. The aircraft was in and out of anvils at 30 kft,
813 then ascended to 36 kft – this part of the flight was fairly rough – apparently the aircraft
814 penetrated the core. At this point the flight was terminated to inspect the aircraft for damage due
815 to the lightning strike.

816 The ER-2 initially flew northeast over the Caribbean into relatively clear air while gaining
817 altitude. The ER-2 then flew southwest along a line with relatively clear air below the aircraft in
818 order to profile aerosol concentrations with its lidar. On this leg, a layer of cirrus was observed in
819 a 12- to 15-km layer. In addition, there was a layer of aerosol extending from the surface to 3 km
820 in the Caribbean. After reaching the southwestern point over the Pacific at about 1320 UT, the
821 ER-2 flew two racetrack patterns in a counter-clockwise pattern in coordination with the DC-8

822 before shifting to a second track for a third rounding. After the DC-8 encountered a lightning
823 strike, the ER-2 was shifted northward to a track that was over a convective core that had a
824 considerable cirrus shield. The ER-2 flew approximately three legs over this core and returned to
825 Costa Rica.

826 827 **5.6 25 July, 2007**

828
829 Figure 13 illustrates the ER-2 flight track on 25 July, 2007. The DC-8 did not fly because
830 damage from the lightning strike on July 24 was being assessed. Low tropopause temperatures
831 were forecast along the coast of Nicaragua, and the goal for the flight was to measure the
832 radiation budget in subvisible cirrus. The ER-2 detected a subvisible cirrus in the low albedo
833 area off the eastern coast of Nicaragua in Figure 13, where GOES did not detect any cloud
834 optical depth. After an initial pass above the cloud, the ER-2 slowly descended through the
835 cloud to make the first measurements of the heating rate in subvisible cirrus. The heating rate is
836 critical to determine if subvisible cirrus pump freeze dried air into the stratosphere. The ER-2
837 also profiled Saharan dust crossing from the Caribbean into the Pacific using the lidar.

838 839 **5.7 28 July, 2007**

840
841 Figure 14 illustrates the flight path of the DC-8 on 28 July, 2007. The ER-2 did not fly due
842 to instrument repair issues. The goal of the DC-8 flight was to profile the Saharan dust layer,
843 and to gain further information about dust removal as air crosses Central America. The DC-8
844 first flew over the Caribbean and identified the dust with lidar, it then descended to sample the
845 dust in situ. A similar flight profile was then flown in the Pacific.

846 847 **5.8 29 July, 2007**

848
849 Figure 15 illustrates the flight tracks for the ER-2 and DC-8 on 29 July, 2007. The goal of
850 these flights was to investigate the microphysical properties of the marine stratus layers off the
851 coast of South America, in order to help CloudSat and CALIPSO better interpret their
852 observations of these clouds. The ER-2 and DC-2 coordinated a flight leg along the coast of
853 South America and under the TERRA overpass, across stratus with varying structure. The ER-2
854 then returned to Costa Rica, while the DC-8 flew through a series of convective cells, one of
855 which was encountered during the CloudSat and CALIPSO overpass. The DC-8 also sampled air
856 in the Gulf of Panama within the radar beam from the Panama ground site.

857 858 **5.10 31 July, 2007**

859
860 Figure 16 illustrates the aircraft flight paths for 31 July, 2007 superimposed on a GOES
861 retrieval of ice water path. The ER-2 and DC-8 first did a series of racetracks over Southern
862 Costa Rica. The goal was to sample the anvil from the large mesoscale complex in the Pacific
863 just off the coast of Costa Rica. Figure 17 provides a view of this mesoscale complex from the
864 DC-8. Following this anvil sampling the ER-2 flew over the convective cores in the complex,
865 then returned to base. Meanwhile the DC-8 proceeded upwind of the complex and did a vertical
866 profile to understand the properties of the materials entering the convection.

867

868 **5.11 3 August, 2007**

869

870 Figure 18 illustrates the flight tracks of the DC-8, ER-2 and WB-57F on 3 August, 2007
871 superimposed on a GOES infrared image. The DC-8 and ER-2 proceeded across Nicaragua,
872 where they met the WB-57F near the border with Honduras. The three aircraft flew through a
873 small convective system. After the WB-57F landed in Costa Rica, the ER-2 and DC-8
874 proceeded to the ground site in Panama, where they sampled the anvils from a convective
875 complex. The DC-8 made a descent over the Panama ground site, while the ER-2 returned to
876 Costa Rica. The DC-8 then sampled the remnants of a convective system over the Pacific, as it
877 followed the CloudSat and CALIPSO overpass track back to Costa Rica.

878

879 **5.12 5 August, 2007**

880

881 Figure 19 illustrates the flight tracks of the DC-8, ER-2 and WB-57F on 5 August, 2007
882 superimposed on a GOES infrared image. The principal goal of this flight was to obtain a
883 vertical profile of cloud properties in the anvil of a convective complex. The three aircraft did a
884 stacked flight in the Pacific near the Gulf of Panama. The ER-2 flew over a convective core near
885 the Panama ground site. After the departure of the other aircraft, the DC-8 did a spiral descent
886 into the boundary layer over the ocean near Columbia to sample the inflowing air to the
887 convective complex. It then flew over the Columbian jungles to sample the air there. Finally it
888 flew over the Panama ground site on its return to Costa Rica.

889

890 **5.13 6 August, 2007**

891

892 Figure 20 illustrates the flight tracks of the DC-8, ER-2 and WB-57F on 6 August, 2007
893 superimposed on a GOES image. The principal goal of this flight was to explore the structure of
894 the TTL as far South of Costa Rica as possible. Some of the flight occurred in subvisible clouds,
895 which were sampled directly by the WB-57F and remotely by the ER-2 and DC-8. The DC-8
896 sampled the boundary layer near the Galapagos Islands, part of which included crossing through
897 a Von Kármán vortex to the north of the Galapagos (Figure 21). The DC-8 returned to Costa
898 Rica along a Terra overpass track.

899

900 **5.14 8 August, 2007**

901

902 Figure 22 illustrates the flight tracks of the DC-8, ER-2 and WB-57F on 8 August, 2007
903 superimposed on a GOES infrared image. The primary goal of this flight was to sample the anvil
904 blowing downwind from a large mesoscale complex in the Pacific Ocean south of Costa Rica. As
905 the anvils evolved the aircraft first made measurements roughly normal to the wind direction,
906 and across the anvils. Later the aircraft were aligned with the wind direction and made
907 measurements along the anvils in increasingly aged air. The WB-57 and DC-8 flew consecutive
908 flight legs through the same anvil cirrus at altitudes of 11.4 and 12 km for comparison of
909 microphysical measurements made on the two platforms. When the WB-57 departed for Costa
910 Rica, the ER-2 flew to a newly developing set of cells and flew over several convective cores.
911 After the return of the ER-2 and WB-57F to Costa Rica, the DC-8 made low-level observations
912 over the rainforest in Columbia. The DC-8 then flew over the Panama ground site on its return
913 to Costa Rica

914

915 **6. Progress towards the TC4 goals**

916

917 The papers in this Special Issue, as well as papers using TC4 data published elsewhere, have
918 helped address many of the TC4 goals. Much data also remains to be analyzed or applied.

919 An important set of questions for the meteorological context of TC4, addressed by *Pfister et*
920 *al.* [2010] are: (1) what are the basic flow patterns in the region, and how typical are those
921 patterns; (2) what is the character of the convection, and how does it compare to previous years;
922 (3) what are the implications of convection and circulation for the origin of air masses sampled
923 during the experiment; and (4) how does the convection and flow vary during the three week
924 period of the experiment?

925 In the TTL, the global circulation is dominated by the Asian Anticyclone, and the easterly
926 winds that persist from the western Pacific to the Atlantic ocean. *Pfister et al.* [2010] find that
927 during TC4, easterly winds were stronger than normal; instead of a weak, fluctuating pattern
928 between easterlies and westerlies over Central America, easterly winds dominated with only
929 occasional interruptions. The August phase of the experiment, in particular, had strong easterlies
930 in the TTL. In the upper troposphere, the character of the flow in the TC4 region is determined
931 by the North American anticyclone, the mid-Atlantic trough and the Central American
932 convective maximum. Though convective divergence was obviously less than normal, the basic
933 flow was similar to previous years.

934 *Pfister et al.* [2010] find that convection was significantly weaker than in previous years,
935 with areas of coldest cloud top temperatures in the Gulf of Panama reduced by upwards of 25%
936 compared to more active years (like 2005). In fact, the incidence of cold cloud tops in the
937 outgoing longwave radiation climatology was among the three lowest out of the 34 years
938 sampled. Though the ENSO cycle, and, to a lesser extent, the Madden-Julian oscillation, played
939 some role in the reduced convective intensity, most of the relatively low frequency of very cold
940 cloud tops in the Gulf of Panama during TC4 cannot be explained by standard large-scale
941 interannual and intrannual tropical variations.

942 The flow patterns and convection determine the origin of the air. An important feature of
943 air at low levels is the strong contribution from flow over the Sahara, reflected in observations of
944 Sahara dust during TC4. *Pfister et al.* [2010] find that in the southern portion of the area
945 surveyed by the aircraft, a significant amount of air originated from the Amazon region. In the
946 upper troposphere, some air was transported from long distances at upper levels and was not
947 directly influenced by convection in the immediate region. Convectively influenced air at
948 200mb came from Central America, the northern Amazon region, the Atlantic ITCZ, and the
949 North American monsoon. Because of the basic easterly pattern, only a limited number of air
950 parcels in the upper troposphere originated from convection in the Eastern Pacific. In the TTL,
951 the basic easterly flow pattern meant that convection to the east, including African and Asian
952 convection, could affect the observed air masses. Near San Jose and northward, African and
953 Asian convection (aged as much as 20 days) may have contributed as much to the air masses as
954 Central and South American convection. South of 8°N, Asian and African convection had far
955 less impact because the easterly flow is weaker.

956 *Pfister et al.* [2010] find there was a strong diurnal cycle in the convection, with the
957 frequency of deepest convection peaking over the oceans at night and in the morning hours.
958 There was variation on longer time scales. The first five days of the experiment were relatively
959 convectively active, with a strong easterly wave pattern. For the next two weeks, easterly waves

960 were relatively weak, and convection was generally less intense. For the last eight days,
961 convection was strong, which coincided with a strong easterly wave pattern.

962 *Dean-Day et al.* [2010], examine the accuracy of the in situ meteorological measurements
963 on the DC-8 and WB-57F. They find that mean DC-8 MMS pressures departed from sonde
964 pressures by up to ± 0.7 mbar using GPS altitude as a common vertical scale, while average
965 temperatures for both the WB-57 and DC-8 MMS agreed to within ± 0.3 K for all comparisons
966 between different aircraft and between aircraft and dropsondes. While mean wind velocity
967 differences were $1.2 - 1.6 \text{ ms}^{-1}$ for all ozonesonde groups, and 1.0 ms^{-1} between MMS
968 instruments on the two aircraft, the difference was $< 0.4 \text{ ms}^{-1}$ between the DC-8 MMS and
969 AVAPS dropsondes. These results demonstrate that newer GPS/INS technology can improve
970 the accuracy of the MMS horizontal wind velocity to $\pm 0.5 \text{ ms}^{-1}$, and confirm the accuracy of
971 MMS pressure and temperature determined in prior investigations. Uncertainties in the accuracy
972 statistics are related to the spatial and temporal separation between platforms, and the
973 apportionment of error between instruments.

974 One group of papers using TC4 data is aimed at questions 1, 2, 3, 6, 7 and 8 in Table 1,
975 better understanding the properties of tropical cirrus clouds, anvils from convective clouds, as
976 well as their impacts on the humidity of the stratosphere and troposphere, and remote sensing.

977 A long-standing controversy about anvil cirrus is the importance of ice crystals with sizes
978 near $10 \mu\text{m}$. During the past decade a number of measurements have indicated that such sized
979 crystals control the optical depths of clouds, and limit their sedimentation rate. However, it has
980 been suggested that these small particles may not actually be so numerous in clouds as thought,
981 but instead many may be created by the shattering of larger particles on the inlets of the sampling
982 instruments. TC4 used instruments that removed many of the surfaces on which shattering might
983 occur, as well as standard instruments on which shattering might have occurred. *Jensen et al.*
984 [2009] show that indeed the vast majority of small particles are measurement artifacts for the
985 clouds observed in TC4. The small particles that do exist contribute little to cloud extinction,
986 radiative forcing, or radiative heating in the anvils.

987 *Lawson et al.* [2010] discussed the size, shape and concentration of ice particles in
988 tropical anvil cirrus and in situ cirrus clouds as measured with a 2D-S probe, an optical imaging
989 probe with improved response characteristics and the ability to remove shattered artifacts. The
990 data were collected with the DC-8 and WB-57F research aircraft near Costa Rica during TC4,
991 and with the DC-8 near Cape Verde during the 2006 NASA African Monsoon Multidisciplinary
992 Analyses (NAMMA) campaign.

993 *Lawson et al.* [2010] collected data in convective turrets, anvils still attached to
994 convection, aged anvils detached from convection and cirrus formed in situ. Unusually strong
995 maritime convection was encountered, with peak updrafts of 20 m s^{-1} , ice water contents
996 exceeding 2 g m^{-3} and total particle concentrations exceeding 10 cm^{-3} at 12.2 km. Ice water
997 contents in the anvils declined outward from the center of convection, decreasing to $< 0.1 \text{ g m}^{-3}$
998 in aged anvil cirrus. The data show that microphysical and radiative properties of both tropical
999 anvils and cirrus are most strongly influenced by ice particles in the size range from about 100 to
1000 $400 \mu\text{m}$. This is contrary to several previous investigations that have suggested that ice particles
1001 less than about $50 \mu\text{m}$ control radiative properties in anvils and cirrus.

1002 *Lawson et al.* [2010] input 2D-S particle area and mass size distributions, plus information
1003 on particle shape, into an optical properties routine that computes cloud extinction, asymmetry
1004 parameter and single scattering albedo. These optical properties were then input into a two-
1005 stream radiative code to compute radiative heating profiles within the various cloud types. The

1006 results produce short- and long-wave heating/cooling vertical profiles in these tropical clouds. A
1007 simple parameterization based on 2D-S measurements is derived from the particle mass size
1008 distribution that yields an area size distribution. The parameterized area size distribution can
1009 then be used in large-scale numerical simulations that include radiative transfer packages.

1010 *Tian et al.* [2009] examined two days of in situ observations of ice particle size spectra in
1011 convectively generated cirrus to determine if the data was well fit to exponential, gamma or
1012 lognormal function size distributions. They showed that transformed exponential, gamma and
1013 lognormal distributions should collapse onto standard curves. An examination of the transformed
1014 spectra, and of deviations of the transformed spectra from the standard curves, shows that the
1015 lognormal function provides the best fit to the observed spectra.

1016 A difficult issue in remote sensing of clouds is to determine the cloud top and base heights,
1017 and to detect multiple cloud layers. Depending on the wavelength and technique used remote
1018 sensing instruments penetrate to different depths. *Hlavka et al.* [2010] addressed this issue using
1019 a lidar and radar on the ER-2. Among other goals they compiled statistical data on cloud
1020 location. *Hlavka et al.* [2010] found that the TC4 Study Area was very cloudy, with clouds
1021 occurring 94% of the time in vertical profiles. One to three cloud layers were common, with the
1022 average calculated at 2.03 layers per profile. The cloud frequency in the upper troposphere
1023 averaged 42%. There were regional differences. The Caribbean had fewer clouds than the other
1024 regions. High clouds occurred over land more frequently than over ocean areas. The Panama
1025 Bight region had the highest probability of clouds throughout the vertical column. The average
1026 height above the ground where the cumulative optical depth (starting at 20 km) reached 1.0 was
1027 5.968 km and where it reached 3.0 was 4.258 km. *Kuji et al.* [2010] in a related study, compare
1028 cloud top altitudes using co-located datasets with Imager, lidar, and Sounder onboard the ER-2.
1029 They discuss the consistency between infrared sounding and lidar backscattering measurements,
1030 and also show a comparison of cloud optical and microphysical properties.

1031 *Selkirk et al.* [2010] discuss balloonsonde measurements of water vapor and ozone using the
1032 University of Colorado Cryogenic Frostpoint Hygrometer and electrochemical concentration cell
1033 (ECC) ozonesondes as well as high-frequency radiosonde measurements made at Alajuela, Costa
1034 Rica [10.0°N, 84.2°W] during the Tropical Convective Systems and Processes mission or TCSP
1035 in July 2005 and TC4. The profiles of water vapor were consistent with the vertical structure of
1036 tropical water vapor in northern summer obtained previously with in situ measurements and with
1037 concurrent Aura MLS, i.e. a broad minimum near 3.2 ppmv between 19 and 20 km and values of
1038 ~6 ppmv at the mean cold point tropopause located close to 16.6 km and 375 K potential
1039 temperature. The profiles also frequently displayed ice supersaturations ranging up to ~140% in
1040 between 12 and 15 km whereas in the immediate vicinity of the cold point tropopause
1041 dehydration is dominant. In two cases from TCSP, dehydration at the coldpoint to values under 3
1042 ppmv were seen.

1043 Time-height sections of radiosonde temperature and wind anomalies reveal coherent
1044 westward-moving wave variations in lower stratosphere extending down to the ~15 km level.
1045 *Selkirk et al.* [2010] found these waves produce temperature fluctuations on the order of ± 7 K in
1046 the stratosphere and are the driver of water vapor variations and dehydration near the tropopause
1047 as well as variations of ozone due to vertical displacements across the strong mean gradient. In
1048 contrast to this wave-driven regime, below the 15 km level – which is approximately the neutral
1049 buoyancy level for deep convection – the waves rapidly weaken with height and water vapor
1050 variations become decoupled from temperature; in this region, the observed supersaturations that
1051 are observed are most likely closely associated with detrainment of deep convective clouds and

1052 anvils. Similarly, the weakening of wave displacements in this convective regime below 15 km
1053 yields a strong decrease in the relative variability of ozone, and vertical mixing is the dominant
1054 process causing ozone variability.

1055 Kucera and Newman [2010] examine the characteristics of convection over the southern
1056 peninsula of Panama and adjacent Gulf of Panama using data from the NASA 10-cm
1057 polarimetric Doppler weather radar (NPOL) and rainfall measurements obtained from a high
1058 resolution rain gauge network. A variety of events were observed during TC4. Events ranged
1059 from short-lived unorganized convection to long-lived mesoscale convective systems (MCSs).
1060 Results show that organized systems often developed and intensified over the Gulf of Panama in
1061 the late evening before weakening and dissipating prior to reaching land in the mid-morning
1062 hours. A secondary peak in convection as a result of strong diurnal heating was observed over
1063 the mountainous region of Panama during mid-afternoon. Analysis of the vertical structure of
1064 the storms was nearly the same for evening and morning with slightly more deep convection in
1065 late afternoon.

1066 An important issue with respect to water is the role of convection in establishing the
1067 water vapor mixing ratio. *Sayres et al.* [2010] report measurements from the ICOS and
1068 HOxotope water isotope instruments and Lyman-alpha hygrometer made during CR-AVE and
1069 TC4 to explore the role convection plays in setting the water vapor mixing ratio of the TTL and
1070 air entering the tropical stratosphere. Isotopologue ratios are heavy compared to the predicted
1071 value based on temperature as the sole control of the water vapor mixing ratio, but are consistent
1072 with convective ice lofting throughout the TTL. Using a convective influence model and a
1073 simple parameterized model of dehydration along back trajectories, *Sayres et al.* [2010] show
1074 that the predominant profile of isotopologue ratios can be explained by convective injection of
1075 isotopically heavy water vapor only into the lower part of the TTL. However, the measurements
1076 clearly show examples of air parcels with significantly enhanced water vapor mixing ratios and
1077 isotopologue ratios as compared to the mean profiles both below and above the summertime
1078 tropical tropopause, though ice particles from convection at these altitudes were not directly
1079 observed during the flight campaigns. The convective influence model shows that these air
1080 parcels were mixed with convective outflow near the Western Tropical Pacific at altitudes lower
1081 than the observations, but still near the local tropical tropopause.

1082 *Kindel et al.* [2010] discuss the important issue of the accuracy of satellite retrieval of
1083 cloud optical properties. They retrieve the cirrus cloud optical depth and effective radius from
1084 hyperspectral irradiance and discrete spectral radiance measurements for four cirrus cloud cases
1085 during TC4 over a range of solar zenith angle (23° to 53°) and high (46-90) and low (5-15)
1086 optical thicknesses. The retrieved optical depth and effective radius using measurements at only
1087 two wavelengths from the Solar Spectral Flux Radiometer (SSFR) Irradiance and the MODIS
1088 Airborne Simulator (MAS) was input to a radiative transfer model using two libraries of ice
1089 crystal single scattering optical properties to reproduce spectral albedo over the spectral range
1090 from 400 to 2130 nm. The two commonly used ice single scattering models were evaluated by
1091 examining the residuals between observed spectral and predicted spectral albedo. The SSFR and
1092 MAS retrieved optical depth and effective radius were in close agreement for the low to
1093 moderately optically thick clouds with a mean difference of 2.76 in optical depth (SSFR lower
1094 relative to MAS) and $2.25 \mu\text{m}$ in effective radius (MAS smaller relative to SSFR). The higher
1095 optical depth case exhibited a larger difference in optical depth (40.5) but nearly identical results
1096 for effective radius. The single scattering libraries were capable of reproducing the spectral
1097 albedo in most cases examined to better than 0.05 for all wavelengths. Systematic differences

1098 between the model and measurements increased with increasing optical thickness and
1099 approached 0.10 between 400-600 nm and selected wavelengths between 1200-1300 nm.
1100 Differences between radiance- and irradiance-based retrievals of optical thickness and effective
1101 radius error sources in the modeling of ice single scattering properties are examined.

1102 Whether clouds absorb more sunlight than would be expected, or not, has been an issue for
1103 many years. *Schmidt et al.* [2010] shed light on this problem using TC4 data. Coordinated flight
1104 legs of the ER-2 and DC-8 aircraft flying above and below extended cirrus layers played an
1105 important part in TC4. The Solar Spectral Flux Radiometer (SSFR) measured up- and downward
1106 irradiance on both aircraft, which allowed the so-called apparent absorption to be determined on
1107 a point-by-point basis along the flight track. Apparent absorption is defined as the difference in
1108 net flux on top and at the bottom of a cloud. It is not a good proxy for the real absorption for
1109 highly heterogeneous cloud scenes where horizontal photon transport through the sides of the
1110 sampling volume is an important contributor to flux divergence. *Schmidt et al.* [2010] show, for
1111 the first time, measured spectral apparent absorption and compare with results from a three-
1112 dimensional radiative transfer model. The modeled cloud field was generated from optical
1113 thickness and effective ice crystal radius retrievals from the MODIS Airborne Simulator (MAS),
1114 and from reflectivity profiles from the Cloud Radar System (CRS), both onboard the ER-2.
1115 *Schmidt et al.* [2010] find considerable apparent absorption in areas of relatively high optical
1116 thickness, for both visible wavelengths (where clouds do not absorb) and in the near-infrared ice
1117 absorption bands. This absorption is well reproduced by the model results. The fact that photons
1118 are effectively re-distributed from optically thick to optically thin regions supports previous
1119 studies where observed absorption biases were attributed to under-sampling of the clear areas
1120 around clouds. The spectral signature of the bias may have implications for cloud remote-
1121 sensing; studying this new effect in greater detail thus appears to be important in future cloud
1122 experiments.

1123 *Eichler et al.* [2010] evaluate the relative impact of ice crystal scattering phase function and
1124 three-dimensional (3D) effects in heterogeneous cirrus clouds on remote-sensing products
1125 (optical thickness and effective crystal radius). Their study is based on 3D and independent pixel
1126 approximation (IPA) radiative transfer model calculations, using an input cloud that was
1127 generated from data collected during TC4. In current ice cloud retrievals from satellite imagers
1128 using unpolarized light, the scattering phase function has to be assumed a-priori. The various
1129 effects of cloud heterogeneities are ignored in current techniques. Both simplifications introduce
1130 errors in the retrievals. *Eichler et al.* [2010] calculated spectral upwelling radiance fields from
1131 the input cloud as they would be sensed from space or aircraft. They thereby used the same ice
1132 cloud properties that are the basis for satellite retrievals from the Moderate Resolution Imaging
1133 Spectroradiometer (MODIS). *Eichler et al.* [2010] then retrieved the optical thickness and crystal
1134 effective radius that would be obtained in standard satellite techniques under the IPA
1135 assumption. The ratios between the retrieved and the original fields are used as a metric for cloud
1136 heterogeneity effects on retrievals. To estimate the error that arises from inappropriate choices of
1137 phase functions, *Eichler et al.* [2010] retrieved optical thickness and crystal effective radius
1138 using different phase functions than the set that was used for calculating the radiance fields. The
1139 ratio between retrieved and original values of optical thickness and effective radius serve as
1140 metric for phase function effects. *Eichler et al.* [2010] then compared the two types of ratios
1141 (heterogeneity effect and scattering phase function effect) and found that both are of the same
1142 magnitude, with different dependencies on optical thickness, effective radius, and optical
1143 thickness variability. *Eichler et al.* [2010] found positive and negative biases of up to 50% for

1144 both optical thickness and crystal effective radius. Cloud heterogeneities cause optical thickness
1145 to be underestimated and effective radius to be overestimated in optically thick regions. The
1146 phase function ratios are constant with cloud optical thickness, but the retrieval bias of effective
1147 radius may increase or decrease with crystal size, depending on the scattering phase function.

1148 *Mace* [2009] used data from the DC-8 underflights in TC4 to help validate the A-Train
1149 sensors. He then found annually averaged cloud properties (occurrence, integrated condensate
1150 mass, effective particle size), cloud radiative effects (cloudy minus clear flux differences at the
1151 top of atmosphere, surface, and in atmosphere), and cloud radiative heating from 20°x20°
1152 latitude-longitude regions in the Southern Ocean centered at 50°S, 135°W and the North Atlantic
1153 centered at 55°N, 25°W using A-Train sensors. *Mace* [2009] found that the study regions
1154 demonstrate a high degree of similarity in cloud occurrence statistics, in cloud properties, and in
1155 the radiative effects of the clouds. Both regions are dominated by a background state of boundary
1156 layer clouds (mean LWP~150 g m⁻³). Boundary layer clouds combined with cirrus (mean IWP
1157 ~100 g m⁻³) amount to approximately 75% of all clouds. Deeper frontal clouds amount to 10-12%
1158 of the coverage. A strong net TOA cooling effect is partitioned between solar cooling of the
1159 surface and IR cooling the atmosphere that is dominated by the ubiquitous boundary layer
1160 clouds. This strong cooling is modulated by upper tropospheric heating in thick cirrus.

1161 *Heymsfield et al.* [2009] compare Doppler radar observations of the strength of vertical
1162 motions in convection from a wide variety of field missions including TC4. They found that
1163 strong updrafts, most exceeding 15 m s⁻¹ with a few exceeding 30 m s⁻¹, are found in all the deep
1164 convection cases, whether over land or ocean. They also found that peak updrafts were almost
1165 always above the 10 km level and in the case of tropical cyclones, closer to the 12 km level. In
1166 addition, tropical convection often has double-peaked updraft velocities with the smaller peak at
1167 lower levels and the larger peak at higher altitudes. Finally, land-based and sea breeze
1168 convection had higher reflectivities, slightly higher vertical velocities, and wider convective
1169 cores than oceanic and tropical cyclone convection. The results are discussed in terms of
1170 dynamical and microphysical implications for numerical models and future remote sensors.

1171 A second group of papers is aimed at questions 4, 5 and 8 in Table 1, trying to understand
1172 transport between the tropical troposphere and the stratosphere, the fates of short-lived
1173 chemicals, ozone chemistry, and remote sensing.

1174 A long-standing issue in TTL science is the rate of transport of materials from the surface
1175 into the lower stratosphere. *Park et al.* [2010] used measurements of CO₂ from the WB-57F to
1176 determine transport rates across the TTL into the lower stratosphere. Based on the distributions
1177 of several species they deduced the local chemical lifetimes due to photolysis and loss by OH
1178 and Cl. They concluded that very short-lived species such as CHCl₃, CH₂Cl₂, and CH₂Br₂, have
1179 much longer local lifetimes at 18-km altitude than air transport time scales, implying that the
1180 species can readily reach the stratosphere even under normal dynamic conditions (i.e., deep
1181 convective events are not required). This result shows that the chlorine- and bromine-containing
1182 very short-lived organic compounds that are not included currently in most models, could
1183 contribute significant amounts of chlorine and/or bromine to the stratospheric loading.

1184 *Bucsela et al.* [2010] present case studies identifying lightning-generated upper-tropospheric
1185 NO_x observed during TC4. Data from DC-8 aircraft missions within and near active storms and
1186 in relatively quiet areas were combine with corresponding data from the Ozone Monitoring
1187 Instrument (OMI) on the Earth Observing System Aura satellite to estimate the lightning-
1188 generated NO₂ (LNO₂) in the observed OMI NO₂ fields near storms. Information on lightning
1189 flashes – primarily cloud-to-ground (CG) flashes – observed by the surface networks operated

1190 by the Instituto Costarricense de Electricidad and the World Wide Lightning Location Network
1191 were examined over storms upwind of regions where OMI data indicates enhanced LNO₂. These
1192 flash data are compared with TRMM/LIS satellite overpass data to obtain the lightning detection
1193 efficiency for total flashes.

1194 *Bucsela et al.* [2010] use the NO₂/NO_x ratio estimated from the NASA Global Modeling
1195 Initiative model, to estimate the average NO_x (NO₂ + NO) production per lightning flash for each
1196 case in their study and obtained production rates of 145 to 636 moles/flash, which are
1197 comparable to or lower than rates derived from cloud-resolved chemistry modeling of storms
1198 observed in mid-latitude experiments. The larger values of production per flash were estimates
1199 for storms in environments with stronger anvil-level winds. LIS flash footprint data that were
1200 available for one of the low-LNO_x production cases with weak upper tropospheric winds
1201 suggests shorter than typical flash lengths for this storm. *Bucsela et al.* [2010] found that
1202 enhancements due to LNO_x over background determined from the OMI data were in general
1203 agreement with those estimated from the in situ aircraft data.

1204 It has long been thought that nitric acid is being depleted in the upper troposphere by
1205 absorption onto ice cloud particle surfaces. *Scheuer et al.* [2010] present new DC-8
1206 measurements of HNO₃ in cirrus clouds from anvil outflow made during TC4. Upper
1207 tropospheric (<9km) measurements made during three flights while repeatedly traversing the
1208 same cloud region revealed depletions of gas-phase HNO₃ in regions characterized by higher ice
1209 water content and surface area. *Scheuer et al.* [2010] speculate that the depleted HNO₃ is due
1210 primarily to adsorption of HNO₃ onto cirrus ice surfaces. Using measurements of cirrus ice
1211 surface area density and some assumptions about background mixing ratios of gas phase HNO₃,
1212 they estimate molecular coverage of HNO₃ on cirrus ice surface in the tropical upper troposphere
1213 during the TC4 racetracks to be about 1×10^{13} molecules·cm⁻². While similar to measurements
1214 made during the NASA CRYSTAL-FACE campaign, this is somewhat less than predicted values
1215 stemming from recent laboratory experiments. *Scheuer et al.* [2010] also presented an
1216 observation of considerably enhanced gas-phase HNO₃ at the base of a cirrus anvil suggesting
1217 vertical redistribution of HNO₃ by sedimenting cirrus particles and subsequent particle
1218 sublimation and HNO₃ evaporation. The impact of released HNO₃, however, appears to be
1219 restricted to a very thin layer just below the cloud.

1220 Isotopes have proven to be important sources of information about the origins and fates of a
1221 number of chemical species in the atmosphere. *Croteau et al.* [2010] discuss vertical profiles of
1222 the oxygen and nitrogen isotopic compositions of N₂O from 500m to 19km from samples
1223 collected from the DC-8 and WB-57F during TC4. These profiles reveal the influence of a
1224 surface source at the lower altitudes and stratospheric photochemistry in the TTL and lower
1225 stratosphere. They are similar to profiles measured during CRAVE in January-February 2006.
1226 The coherent, predictable patterns measured show that, despite the large and often confounding
1227 variability in N₂O isotopic compositions on the scale of soil chamber or ocean sample
1228 measurements, these and future vertical profiles of N₂O isotopic compositions even at current
1229 measurement precisions can be used to constrain the N₂O isotope budget and the biogeochemical
1230 cycling of N₂O.

1231 *Avery et al.* [2010] examine the DC-8 in situ data from sampling in active convection and
1232 find a significant anti-correlation between in situ ozone and cloud water content. Further, since
1233 there is little variability in boundary layer ozone in the convective donor region while there is a
1234 vertical gradient in ozone, low ozone in the upper troposphere can be used as a tracer for

1235 convective transport.. The tracers peroxyacetic acid (negative) and methyl hydrogen peroxide
1236 and bromine (positive) substantiate the results from using ozone as a tracer.

1237 Two case studies are shown by *Avery et al.* [2010] to demonstrate the ozone/cloud particle
1238 relationship, and then statistical distributions from all the available data in the upper troposphere
1239 are used to estimate the amount of convective turnover that has occurred below the tropical
1240 tropopause transition layer. The estimated amount of convective turnover is 50% in this region
1241 of the ITCZ, with the average height of convective outflow determined by a statistical minimum
1242 in the aggregate ozone profiles occurring at about 10 km. It appears that convective lofting in
1243 this region of the ITCZ is a two-stage process that mixes boundary layer air (ozone ~ 20 ppbv)
1244 up to an outflow region at 3-5 km, and then entrains air at 3-5 km and rapidly transports it to an
1245 outflow region located near 10 km.

1246 *Petropavlovskikh et al.* [2009] found that very low ozone values were sometimes observed
1247 in the TTL during TC4. They examined the DC-8 in situ data and the remotely sensed data
1248 above the aircraft and found the TTL to be influenced by both slow ascent and by rapid transport
1249 due to deep convection. The transport trajectories and correlated measurements of ozone and
1250 boundary layer tracers suggest a strong connection between the deep convective processes
1251 regularly observed at low northern latitudes in July 2007 and the low-ozone episodes observed in
1252 the TTL near the coast of Ecuador. Back trajectory analyses indicate that the low ozone features
1253 observed near the coast of Ecuador in the CAFS integrated ozone column and the DIAL ozone
1254 profile measurements aboard of the NASA DC-8 aircraft in July of 2007 are influenced by air
1255 with an origin at the south border of Mexico. Because the ozone feature is so pronounced after
1256 an estimated 8 days of transit in the upper troposphere, it may provide information on mixing
1257 time scales in the TTL. Similar low ozone values in the TTL were seen in DIAL data during the
1258 PEM-A and PEM-B campaigns, however previous observations have not noted the low ozone
1259 "blobs" or "bubblers" seen during TC4.

1260 The ozonesondes from the SHADOZ sites at Costa Rica and San Cristobal (1.0S, 99W),
1261 along with daily launches from the NATIVE Panama location (7.8N, 80W), provided a fixed-site
1262 perspective for viewing ozone structure in the TTL. The mean ozone profiles in the upper
1263 troposphere and lower TTL from Costa Rica and Panama display the characteristic "S-shape" of
1264 most tropical SHADOZ sites [e.g., *Folkins et al.*, 2002] that was also observed over Mexico City
1265 during August 2006 [*Thompson et al.*, 2008]. The low ozone segment corresponds to cloud
1266 outflow levels detected during TC4 sampling, e.g. with the ER-2 CPL and CRS imagery [*Hlavka*
1267 *et al.*, 2010], as well as tracers from the DC-8. Analysis of stable ozone laminae in the Costa
1268 Rican and Panama sondes revealed a persistent pattern of convectively generated equatorial
1269 waves in the TTL [Figure 4 in *Thompson et al.*, 2010].

1270 *Morris et al.* [2010] present interesting observations of a strong convective cell formed in
1271 the Gulf of Panama east of Las Tablas on the morning of Sunday, 5 August 2007. World Wide
1272 Lightning Location Network data indicated 485 lightning flashes associated with this cell
1273 between 0800 and 1700 UT, with 398 of those flashes between 1200 and 1500 UT. At 1505 UT
1274 that day, an ozonesonde ascended into the southern edge of the now dissipating convective cell
1275 as it came ashore from the east and moved west across the Azuero Peninsula of Panama. Due to
1276 condensation on the balloon, down drafts associated with the cell, or a combination of both, the
1277 balloon ascended through the 2- to 5-km region 5 times between 1512 and 1700, providing a
1278 truly unique examination of ozone production inside of a convective cell. Ozone concentrations
1279 at these altitudes increased 4 – 12 ppb over the 108 minutes between the first and last ascent
1280 through these layers, yielding ozone production rates of 3 – 10 ppb/hr and (assuming uniform

1281 production throughout the convective cell) $\sim 2 \times 10^6$ moles of ozone. Using a photochemical
1282 model and data from the ER-2, WB-57, and DC-8, all of which flew in the vicinity of this
1283 convective cell, *Morris et al.* [2010] are able to simulate the ozone production calculated using
1284 the balloon data.

1285 *Thornberry et al.* [2010] investigated the composition of aerosol residuals after heating to
1286 300°C. The PALMS single particle mass spectrometer analyzed the composition of the
1287 nonvolatile fraction of the aerosols in a number of environments studied in TC4. The marine
1288 boundary layer, the free troposphere and the continental boundary layer over the Columbian
1289 jungle were studied. Sulfates were completely driven off by heating, except for sodium sulfate
1290 and related compounds in sea salt. Organic material in marine aerosols was less volatile than
1291 chlorine. Biomass aerosols survived heating better than sulfate-organic particles. For all of the
1292 particles there was a significant carbonaceous contribution other than elemental carbon.

1293

1294 7. Summary

1295

1296 TC4 addressed each of the goals it set out to consider (Table 1). Within the context of
1297 related missions and NASA's satellite program, we are significantly closer to answering some of
1298 these fundamental questions. While the late arrival of the WB-57F compromised our ability to
1299 obtain as much high altitude in situ data as we originally planned, we were fortunate that the DC-
1300 8 had a sophisticated instrument package and was able to meet many of the goals originally set
1301 for the WB-57F. We were able to make three flights with the set of three aircraft, which did
1302 provide a considerable amount of useful data over the full range of altitudes.

1303 The execution of the TC4 field mission was a significant advance over many previous
1304 missions because of our ability to control the aircraft in real time. We often changed the flight
1305 plans so that the aircraft we able to sample convective systems as they evolved. It was common
1306 for the locations of convective complexes to be significantly different between the forecasts and
1307 reality, for example for convection to be in the Pacific rather than in the Caribbean. These
1308 differences required us to alter flight plans in significant ways just after takeoff. In addition,
1309 convective cores can appear within minutes, and convective complexes dissipate over time.
1310 Therefore, we had to alter flight plans in real time to keep the aircraft away from dangerous
1311 portions of the clouds, but also to take data in the interesting portions of the clouds such as
1312 anvils. We also were able to use data from the aircraft in real time to maximize the locations of
1313 the aircraft relative to interesting phenomena. For example, by using lidar data showing the
1314 locations of cloud and aerosol layers, we were able to alter the aircraft altitude to probe these
1315 layers, which normally would not have been identified until after the mission. The ability to
1316 control the aircraft in flight has been developing for some time, but this is the first mission in
1317 which the three NASA aircraft had mechanisms to track all of them, and to downlink data. This
1318 advance converts aircraft research into an experimental framework, in which questions can be
1319 asked and addressed in real time and phenomena probed in greater detail than before when they
1320 were identified only in forecasts.

1321

1322 **Acknowledgments.** We thank the aircraft managers, engineers and ground crews of all the
1323 aircraft that participated in TC4. We particularly thank the pilots of the ER-2, David Wright,
1324 Denis Steele and DeLewis Porter and Mobile Pilot Jan Nystrom, the WB-57F pilots Rob Rivers,
1325 Scott Reagan and William Rieke and Backseaters, John Bain, Dominic Del Russo and Joseph
1326 Gerky; and the DC-8 pilots William Brocket, Mike Fuller, Manny Puerta and the late Edwin

1327 Lewis. The ER-2 aircraft and pilots were very well supported by the personnel of NASA's
1328 Dryden Flight Research Center Airborne Science Directorate, the WB-57F by NASA's Johnson
1329 Space Center High Altitude Research Program and the DC-8 by the University of North
1330 Dakota's National Science Education Research Center. We thank the ER-2 aircraft Program
1331 Director, Robert Curry, the DC-8 Program Director, Rick Shetter and the WB-57F Program
1332 Manager, Ken Cockrell. We also thank the ER-2 aircraft coordinators Jacques Vachon, and
1333 Mike Kapitzke; the DC-8 Aircraft Manager Steve Davis, and the DC-8 Mission Manager Dave
1334 Easmunt; and the WB-57F Program Engineers Shelly Baccus and Frank Caldeiro, the Mission
1335 Manager William (Bud) Meins, and the Integration Manager, Marty Ross, as well as the all of
1336 the aircraft crews. The NASA Ames Earth Science Project Office made tremendous
1337 contributions to the operations and overall success of TC4. Our special thanks go to Kent
1338 Schiffer, Mike Gaunce, Sue Tolley, Quincy Allison, Dan Chirica, and the late Steve Gaines. We
1339 also appreciate the support of the NPOL radar, NATIVE trailer and Sat Com groups in Panama
1340 the SMART mobile radar in Costa Rica. . We thank the RTMM and REVEAL teams from
1341 NASA Marshall Earth Science Office and NASA Dryden Test Systems Directorate, respectively,
1342 for enabling the collection and display of airborne and ground-based data sets, which supported
1343 mission planning and enabled critical real time decision making. The shipment of the tons of
1344 science hardware to San Jose Costa Rica could not have been accomplished without the
1345 tremendous efforts of the U.S. Air Force Material Command. We would also like to thank the
1346 pilots and staff of the NASA C-9, NASA G-3 and Beale Air force Base KC-135 for all their
1347 support. We would like to record our special appreciation and thanks to Kathy Thompson for her
1348 dedication and effort throughout the planning, operation, and post-mission analysis of TC4.
1349 Kathy was ably assisted by Rose Kendall, to whom we also send our thanks. Tommy
1350 Thompson's myriad skills were critical to the successful operation of the mission in the field.
1351 We thank him for being there to make sure, once again, that it all worked. The airport personnel
1352 at Juan Santamaria airport were very helpful to the mission. The various Costa Rican
1353 government, academic and commercial organizations we worked with, including CeNAT,
1354 DGAC, Alterra, ICE, IMN, ADS, and the Servicio de Vigilancia Aerea were invaluable. The
1355 same can be said for the Panamanian government and academic organizations. The Costa Rican
1356 National Center for Advanced Technology (CENAT), and especially Oliver Gómez, were
1357 instrumental in logistical support, both before and during the mission. The meteorological
1358 forecasting team in Costa Rica was critical to the success of TC4. This was a joint effort of the
1359 Instituto Meteorológico Nacional (IMN), the Centro de Investigaciones Geofísicas (CIGEFI) at
1360 the University of Costa Rica and the Instituto Costarricense de Electricidad (ICE). IMN team
1361 members were Evelyn Quirós Badilla, Gustavo Murillo Zumbado and Eladio Solano León; the
1362 CIGEFI group, under the direction of Prof. Jorge Amador, included Erick Rivera Fernández,
1363 Marcela Ulate Medrano, Ana María Duran Quesada and Blanca Calderón Solera; and Berny
1364 Fallas López represented ICE. NASA Headquarters management and Program Managers
1365 supported this mission in many meaningful ways. The US Embassies in Costa Rica and Panama
1366 were especially helpful in coordinating this effort. We appreciate the hospitality of Costa Rican
1367 Ambassador Mark Langdale. We appreciate the help of the people of Panama who facilitated the
1368 use of the NATIVE trailer and the NPOL radar, and the people of the Galapagos who helped
1369 with balloon launching. We especially thank the President and people of Costa Rica, who
1370 reconstructed the hangar used by the WB-57F, loaned us the President's hangar for the ER-2 and
1371 were very friendly, helpful and hospitable.

1372

1373 **Reference List**

- 1374 Avery, M., J. Joiner, C. Twohy, G. Diskin, G. Sachse, P. Lawson, M. McGill, K. Severance
1375 (2010), Convective Distribution of Tropospheric Ozone and Tracers in the Central American
1376 ITCZ Region: Evidence from Observations During TC4, *J. Geophys. Res.* submitted to this
1377 special issue.
- 1378 Boehm, M. T., and J. Verlinde (2000), Stratospheric influence on upper tropospheric tropical
1379 cirrus, *Geophys. Res. Lett.*, *27*, 3209-3212.
- 1380 Bucsela, E., et al. (2010), Lightning-generated NO_x seen by OMI during NASA's TC4
1381 experiment, *J. Geophys. Res.*, submitted to this special issue.
- 1382 Comstock, J. M., T. P. Ackerman, and G. G. Mace (2002), Ground based remote sensing of
1383 tropical cirrus clouds at Nauru island: Cloud statistics and radiative impacts, *J. Geophys. Res.*,
1384 *107*, D234714 , doi:10.1029/2002JD002203.
- 1385 Corti, T., B. P. Luo, Q. Fu, H. Vömel, and T. Peter (2006), The impact of cirrus clouds on
1386 tropical troposphere-to-stratosphere transport, *Atmos. Chem. Phys.*, *6*, 2539–2547.
- 1387 Corti, T., et al. (2008), Unprecedented evidence for deep convection hydrating the tropical
1388 stratosphere, *Geophys. Res. Lett.*, *35*, L10810, doi:10.1029/2008GL033641.
- 1389 Croteau, P., E. Atlas, S. M Schauffler, D. R Blake and K. A. Boering (2010), The effects of local
1390 and regional sources on the isotopic composition of nitrous oxide in the tropical free
1391 troposphere and tropopause layer, *J. Geophys. Res.*, this special issue.
- 1392 Dean-Day, J., T.P. Bui, H. Vömel. C. Chang and E. Korn, (2010), An evaluation of MMS
1393 pressure, temperature and horizontal wind accuracy, *J. Geophys. Res.*, this special issue.
- 1394 DeMott, P.J., K. Sassen, M.R. Poellet, D. Baumgardner, D.C. Rogers, S.D. Brooks, A.J. Prenni,
1395 and S.M. Kreidenweis (2003), African dust aerosols as atmospheric nuclei, *Geophys. Res.*
1396 *Lett.* *30*, 1732, doi:10.1029/2003GL017410.
- 1397 Dessler, A. E., T. F. Hanisco, and S. Fueglistaler (2007), Effects of convective ice lofting on H₂
1398 O and HDO in the tropical tropopause layer, *J. Geophys. Res.*, *112*, D18309,
1399 doi:10.1029/2007JD008609.
- 1400 Dvortsov, V.L.M.A. Geller, S. Solomon, S.M. Schauffler, M. Sue, E.L. Atlas, and D.R. Blake
1401 (1999), Rethinking halogen budgets in the midlatitude lower stratosphere, *Geophys. Res. Lett.*,
1402 *26*, 1699-1702, 1999.
- 1403 Eichler, H., S. Schmidt, R. Buras, M. Wendisch, P. Pilewskie, B. Mayer, M. King, L. Tian, and
1404 G. Heymsfield (2010), The relative impact of cloud heterogeneities and scattering phase
1405 function on remotely sensed cirrus optical thickness and effective crystal radius, *J. Geophys.*
1406 *Res.*, submitted to this special issue.
- 1407 Folkins, I., M. Loewenstein, J. Podolske, S. J. Oltmans and M. Proffitt (1999), A barrier to
1408 vertical mixing at 14 km in the tropics: Evidence from ozonesondes and aircraft
1409 measurements, *J. Geophys. Res.*, *104*, 22,095-22,102.
- 1410 Folkins I., P.O. Wennberg, T.F. Hanisco, J.G. Anderson and R.J. Salawitch (1997), OH, HO₂,
1411 and NO in two biomass burning plumes - sources of HO_x and implications for ozone
1412 production, *Geophys. Res. Lett.*, *24*, 3185-3188.
- 1413 Folkins, I., C. Braun, A. M. Thompson, J. C. Witte (2002), Tropical ozone as in indicator of deep
1414 convective outflow, *J. Geophys. Res.*, **107**, D13, doi: 10.1029/2001JD001178.
- 1415 Fridlind, A.M., A. S. Ackerman, E.J. Jensen (2004), Evidence for the predominance of mid-
1416 tropospheric aerosols as subtropical anvil cloud nuclei, *Science*, *304*, 718-722.
- 1417 Fueglistaler, S., and P. H. Haynes (2005), Control of interannual and longer-term variability of
1418 stratospheric water vapor, *J. Geophys. Res.*, *110*, doi:10.1029/2004JD006,019.

1419 Fueglistaler, S., A. E. Dessler, T. J. Dunkerton, I. Folkins, Q. Fu, and P. W. Mote (2008), The
1420 tropical tropopause layer, *Rev. Geophys.*, *110*(D08107), doi:10.1029/2004JD005,516.

1421 Gao, R.S., et al. (2004), Evidence that nitric acid increases relative humidity in low-temperature
1422 cirrus clouds, *Science*, *303*, 516-520.

1423 Gettelman, A. and P. M. de F. Forster (2002), A climatology of the tropical tropopause layer, *J.*
1424 *Met. Soc. Japan*, *80*, 911-924.

1425 Gettelman, A., W. J. Randel, F. Wu, and S. T. Massie (2002), Transport of water vapor in the
1426 tropical tropopause layer, *Geophys. Res. Lett.*, *29*(1009), 10.1029/2001GL013818.

1427 Gettelman, A., P. M. de F. Forster, M. Fujiwara, Q. Fu, H. Vömel, L. K. Gohar, C. Johanson, and
1428 M. Ammerman (2004), Radiation balance of the tropical tropopause layer, *J. Geophys. Res.*,
1429 *109*, doi:1029/2003JD004,190.

1430 Hartmann, D. L., J. R. Holton, and Q. Fu (2001), The heat balance of the tropical tropopause,
1431 cirrus, and stratospheric dehydration, *Geophys. Res. Lett.*, *28*, 1969–1972.

1432 Heymsfield, G.M., L. Tian, A. J. Heymsfield, L. Li, and S. Guimond (2009), Characteristics of
1433 deep tropical and sub-tropical convection from nadir-viewing high-altitude airborne Doppler
1434 radar, *J. Atmos. Sci.*, in press.

1435 Highwood, E. J. and B. J. Hoskins (1998), The tropical tropopause, *Quart. J. Roy. Meteor. Soc.*,
1436 *124*, 1579-1604.

1437 Hlavka, D., L. Tian, W. Hart, L. Li, M. McGill, and G. Heymsfield (2010), Vertical cloud
1438 climatology during TC4 derived from high-altitude aircraft merged lidar and radar, *J.*
1439 *Geophys. Res.*, this special issue.

1440 Holton, J., and A. Gettelman (2001), Horizontal transport and dehydration of the stratosphere,
1441 *Geophys. Res. Lett.*, *28*, 2799–2802.

1442 Jacob, D.J., J.H. Crawford, M. M. Kleb, V. S. Connors, R. J. Bendura, J. L. Raper, G. W. Sachse,
1443 J. C. Gille, L. Emmons, and C. L. Heald (2003), The Transport and Chemical Evolution over
1444 the Pacific (TRACE-P) aircraft mission: design, execution, and first results, *J. Geophys. Res.*,
1445 *108* (D20), 8781, 10.1029/2002JD003276.

1446 Jaeglé, L., D. J. Jacob, P. O. Wennberg, C. M. Spivakovsky, T. F. Hanisco, E. L. Lanzendorf, E.
1447 J. Hintsa, D. W. Fahey, E. R. Keim, M. H. Proffitt, E. Atlas, F. Flocke, S. Schauffler, C. T.
1448 McElroy, C. Midwinter, L. Pfister, and J. C. Wilson (1997), Observed OH and HO₂ in the
1449 upper troposphere suggest a major source from convective injection of peroxides, *Geophys.*
1450 *Res. Lett.*, *24*, 3181-3184.

1451 Jenkins G. S., K. Mohr, V. R. Morris, and O. Arino (1997), The role of convective processes
1452 over the Zaire-Congo basin to the southern hemispheric ozone maximum, *J. Geophys. Res.*,
1453 *102*, 8963-8980.

1454 Jensen, E. J., and L. Pfister (2004), Transport and freeze-drying in the tropical tropopause layer,
1455 *J. Geophys. Res.*, *109*(D02207), doi:10.1029/2003JD004022.

1456 Jensen, E. J., D. Starr, and O. B. Toon (2004), Mission investigates tropical cirrus clouds, EOS
1457 Trans. AGU, 85, 45-50.

1458 Jensen, E. J., A. S. Ackerman, and J. A. Smith (2007), Can overshooting convection dehydrate
1459 the tropical tropopause layer?, *J. Geophys. Res.*, *112*, D11209, doi: 10.1029/2006JD007943.

1460 Jensen, E. J., O. B. Toon, H. B. Selkirk, J. D. Spinhirne, and M. R. Schoeberl (1996), On the
1461 formation and persistence of subvisible cirrus clouds near the tropical tropopause, *J. Geophys.*
1462 *Res.*, *101*, 21,361–21,375.

1463 Jensen, E. J., et al. (2005), Ice supersaturations exceeding 100% at the cold tropical tropopause:
1464 implications for cirrus formation and dehydration, *Atmos. Chem. Phys.*, *5*, 851–862.

1465 Jensen, E. J., et al. (2008), Formation of large (100 μm) ice crystals near the tropical tropopause,
1466 *Atmos. Chem. Phys.*, *8*, 1621-1633.

1467 Jensen, E. J. et al. (2009), On the importance of small ice crystals in tropical anvil cirrus, *Atmos.*
1468 *Chem. Phys. Discuss*, *9*, 5321-5370.

1469 Kindel, B. C., K. Sebastian, P. Pilewskie, B. Baum, P. Yang, and S. Platnick (2010),
1470 Observations and modeling of cirrus shortwave spectral albedo during the Tropical
1471 Composition, Cloud and Climate Coupling Experiment, *J. Geophys. Res.*, submitted to this
1472 special issue.

1473 Kley, D., P. J. Crutzen, H. G. J. Smit, H. Vömel, S. J. Oltmans, H. R. Grassl, and V. Ramanathan
1474 (1996), Observations of near-zero ozone concentrations over the convective Pacific - effects
1475 on air chemistry, *Science*, *274*, 230-233.

1476 Ko, M.K.W. and G. Poulet (2002), Chapter 2. Very-Short Halogen and Sulfur Substances,
1477 *Scientific Assessment of Ozone Depletion: 2002*, WMO/UNEP.

1478 Ko M.K.W., N. D. Sze, C. J. Scott, and D. K. Weisenstein (1997), On the relation between
1479 stratospheric chlorine/bromine loading and short-lived tropospheric source gases, *J. Geophys.*
1480 *Res.*, *102*, 25507-25517.

1481 Komhyr, W. D., R. A. Barnes, G. B. Brothers, J. A. Lathrop, and D. P. Opperman (2008),
1482 Electrochemical concentration cell ozonesonde performance during STOIC, *J. Geophys. Res.*,
1483 *100*, 9231– 9244.

1484 Kramer, M., et al. (2009), Ice supersaturations and cirrus cloud crystal numbers, *Atmos. Chem.*
1485 *Phys.*, *9*, 3505-3522.

1486 Kucera, P., and A. J. Newman (2010), Characteristics of convection observed over Panama and
1487 adjacent Gulf of Panama during TC4, *J. Geophys. Res.*, submitted to this special issue.

1488 Kuji, M., S. Platnick, M.D. King, G. T. Arnold, G. Wind, M. McGill, W. D. Hart, D. L. Hlavka,
1489 and R. E. Holz (2010), Comparison of cloud top altitudes from passive and active remote
1490 sensors onboard ER-2 during TC4, *J. Geophys. Res.* Submitted to this special issue.

1491 Lawson, R. P., E. J. Jensen, D. L. Mitchell, B. Baker, Q. Mo, and B. Pilon (2010),
1492 Microphysical and radiative properties of tropical clouds investigated in TC4 and NAMMA,
1493 *J. Geophys. Res.*, this special issue.

1494 Liu, C., and E. J. Zipser (2005), Global distribution of convection penetrating the tropical
1495 tropopause, *J. Geophys. Res.*, *110*, doi:10.1029/2005JD006,063.

1496 Logan, J. A. (1999), An analysis of ozonesonde data for the troposphere: Recommendations for
1497 testing 3-D models, and development of a gridded climatology for tropospheric ozone, *J.*
1498 *Geophys. Res.*, *104*, 16,115-16,149.

1499 Luo, Z. and W. B. Rossow (2004), Characterizing tropical cirrus life cycle, evolution, and
1500 interaction with upper-tropospheric water vapor using Lagrangian trajectory analysis of
1501 satellite observations, *J. Climate*, *17*, 4541-4564.

1502 Mace, G. G., M. Deng, B. Soden and E Zipser (2005), Association of tropical cirrus in the 10-15
1503 km layer with deep convective sources: An observational study combining millimeter radar
1504 data and satellite-derived trajectories, *J. Atmos. Sci.*, *63*, 480-503.

1505 Mace, G. G. (2009), Cloud properties and radiative forcing over the maritime storm tracks of the
1506 Southern Ocean and the North Atlantic derived from A-Train, *J. Geophys. Res.*, submitted
1507 2009.

1508 McFarquhar, G. M., A. J. Heymsfield, J. Spinhirne, and B. Hart (2000), Thin and subvisual
1509 tropopause cirrus: Observations and radiative impacts, *J. Atmos. Sci.*, *57*, 1841–1853.

1510 McKeen S.A., T. Gierczak, J. B. Burkholder, P. O. Wennberg, T. F. Hanisco, E. R. Keim, R. S.
1511 Gao, S. C. Liu, A. R. Ravishankara, D. W. Fahey (1997), The photochemistry of acetone in

1512 the upper troposphere - a source of odd-hydrogen radicals, *Geophys. Res. Lett.*, *24*, 3177-
1513 3180.

1514 Morris, G. (2010), Observations of ozone production in a dissipating tropical convective cell
1515 during TC-4, *J. Geophys. Res.*, submitted this special issue.

1516 Mote, P. W., K. H. Rosenlof, M. E. McIntyre, E. S. Carr, J. C. Gille, J. R. Holton, J. S.
1517 Kinnersley, H. C. Pumphrey, J. M. Russell, and J. W. Waters (1996), An atmospheric tape
1518 recorder: The imprint of tropical tropopause temperatures on stratospheric water vapor, *J.*
1519 *Geophys. Res.*, *101*, 3989–4006.

1520 Murphy, D. M., D. W. Fahey, M.H. Proffitt, S. C. Liu, K. R. Chan, C. S. Eubank, S.R. Kawa,
1521 and K. K. Kelly (1993), Reactive nitrogen and its correlation with ozone in the lower
1522 stratosphere and upper troposphere, *J. Geophys. Res.*, *98*, 8751-8773.

1523 Newman, P. A. (2002), An overview of the SOLVE/THESEO 2000 campaign, *J. Geophys. Res.*,
1524 *107*, 8529, doi: 10.1029/2001JD001303.

1525 Niwano, M., K. Yamazaki, and M. Shiotani (2003), Seasonal and QBO variations of the ascent
1526 rate in the tropical lower stratosphere as inferred from UARS HALOE trace gas data, *J.*
1527 *Geophys. Res.*, *108*, doi:1029/2003JD003871.

1528 Oltmans, S. J., et al. (2001), Ozone in the Pacific troposphere from ozonesonde observations, *J.*
1529 *Geophys. Res.* *106*, 32,501-32,526.

1530 Park, S., et al. (2007), The CO₂ tracer clock for the Tropical Tropopause Layer, *Atmos. Chem.*
1531 *Phys.*, *7*, 3989–4000.

1532 Park, S., et al. (2010), Vertical transport rates for the Tropical Tropopause Layer from
1533 observations of CO₂: Implications for distributions of lone- and short-lived chemical
1534 compounds, *J. Geophys. Res.* This special issue.

1535 Petropavlovskikh, I. et al. (2010), Low ozone bubbles observed in the TTL during the TC4
1536 campaign in 2007, *J. Geophys. Res.* This special issue.

1537 Pfeilsticker, K., W. T. Sturges, H. Bosch, C. Camy-Peyret, M. P. Chipperfield, A. Engel, R.
1538 Fitzenberger, M. Muller, S. Payan, and B. M. Sinnhuber (2000), Lower stratospheric organic
1539 and inorganic budget for the Arctic winter 1998/99, *Geophys. Res. Lett.*, *27*, 3305-3308.

1540 Pfister, L., H. B. Selkirk, D. O’C. Starr, P. A. Newman, and K. H. Rosenlof (2010), A
1541 meteorological overview of the TC4 mission, *J. Geophys. Res.*, this special issue.

1542 Randel, W. J., F. Wu, S. J. Oltmans, K. Rosenlof, and G. E. Nedoluha (2004), Interannual
1543 changes of stratospheric water vapor and correlations with tropical tropopause temperatures,
1544 *J. Atmos. Sci.*, *61*, 2133-2148.

1545 Rosenlof, K. H. and J. R. Holton (1993), Estimates of the stratospheric residual circulation using
1546 the downward control principle, *J. Geophys. Res.*, *98*, 10,465-10,479.

1547 Rosenlof, K. H., A. F. Tuck, K. K. Kelly, J. M. Russell, and M. P. McCormick (1997),
1548 Hemispheric asymmetries in water vapor and inferences about transport in the lower
1549 stratosphere, *J. Geophys. Res.*, *102*, 13,213–13,234.

1550 Sayres, D.S., J. M. St. Clair, T. F. Hanisco, E. J. Moyer, A. S. O’Brien, J. B. Smith, E. M.
1551 Weinstock, J. G. Anderson, L. Pfister, M. Legg. (2010), The influence of convection on the
1552 water isotopic composition of the TTL and the tropical stratosphere, *J. Geophys. Res.*,
1553 submitted to this special issue.

1554 Scheuer, E., J.E. Dibb, C. Twohy, D. C. Rogers, A. J. Heymsfield, and A. Bansemmer (2010),
1555 Evidence of nitric acid uptake in warm cirrus clouds during the NASA TC4 campaign, *J.*
1556 *Geophys. Res.*, this special issue.

1557 Schmidt, K. S., P. Pilewskie, B. Kindel, S. Platnick, M. King, G. Wind, G. T. Arnold, L. Tian,
1558 M. Wendisch (2010), Apparent and real absorption of solar spectral irradiance in
1559 heterogeneous clouds, *J. Geophys. Res.*, submitted to this special issue.

1560 Schoeberl, M. R., A. R. Douglass, R. S. Stolarski, S. Pawson, S. E. Strahan, and W. Read (2008),
1561 Comparison of lower stratospheric tropical mean vertical velocities, *J. Geophys. Res.*, *113*,
1562 doi:10.1029/2008JD010,221.

1563 Schultz, M. G., et al. (1999), On the origin of tropospheric ozone and NO_x over the tropical
1564 Pacific, *J. Geophys. Res.* *104*, 5829-5843.

1565 Selkirk, H. B., H. Vömel, J. Valverde, L. Pfister (2010), The detailed structure of the tropical
1566 upper troposphere as revealed by balloonsonde observations of water vapor, ozone,
1567 temperature and winds during the NASA TCSP and TC4 campaigns, *J. Geophys. Res.*

1568 Staudt, A.C., D. J. Jacob, J. A. Logan, D. Bachiochi, T. N. Krishnamurti, and N. Poisson (2002),
1569 Global chemical model analysis of biomass burning and lightning influences over the South
1570 Pacific in austral spring, *J. Geophys. Res.*, *107*, 4200, doi: 10.1029/2000JD000296.

1571 Staudt, A.C., D. J. Jacob, F. Ravetta, J. A. Logan, D. Bachiochi, T. N. Krishnamurti, S.
1572 Sandholm, B. Ridley, H.B. Singh, and B. Talbot (2003), Sources and chemistry of nitrogen
1573 oxides over the tropical Pacific, *J. Geophys. Res.*, *108*, 8239, doi: 10.1029/2002JD002139.

1574 Strahan S.E. (1999), Climatologies of lower stratospheric NO_y and O₃ and correlations with N₂O
1575 based on in situ observations, *J. Geophys. Res.*, *104*, 30463-30480.

1576 Thompson, A. M., K. E. Pickering, D. P. McNamara, M. R. Schoeberl, R. D. Hudson, J. H. Kim,
1577 E. V. Browell, V. W. J. H. Kirchoff, and D. Nganga (1996), Where did tropospheric ozone
1578 over southern Africa and the tropical Atlantic come from in October, 1992? Insights from
1579 TOMS, GTE/TRACE-A and SAFARI-92, *J. Geophys. Res.*, *101*, 24,251-24,278.

1580 Thompson, A. M., J. C. Witte, S. J. Oltmans, F. J. Schmidlin, J. A. Logan, M. Fujiwarra, V.
1581 Kirchhoff, F. Posny, G. Coetzee, B. Hoegger, S. Kawakami, and T. Ogawa (2003a), The
1582 1998-2000 SHADOZ (Southern Hemisphere Additional Ozonesondes) tropical ozone
1583 climatology: Stratospheric and tropospheric variability and the zonal wave-one, *J. Geophys.*
1584 *Res.*, *108*, (D2), 8241, doi:10.1029/2002JD002241.

1585 Thompson, A. M., et al. (2003b), Southern Hemisphere Additional Ozonesondes (SHADOZ)
1586 1998-2000 tropical ozone climatology. 1. Comparison with TOMS and ground-based
1587 measurements, *J. Geophys. Res.*, *108*, 8238, doi: 10.1029/2001JD000967.

1588 Thompson, A. M., J. E. Yorks, S. K. Miller, J. C. Witte, K. M. Dougherty, G. A. Morris, D.
1589 Baumgardner, L. Ladino, B. Rappenglueck (2008), Tropospheric ozone sources and wave
1590 activity over Mexico City and Houston during MILAGRO/Intercontinental Transport
1591 Experiment (INTEX-B) Ozonesonde Network Study, 2006 (IONS-06), *Atmos. Chem. Phys.*,
1592 *8*, 5113-5126.

1593 Thompson, A. M., A.M. Luzik, G. A. Morris, J. E. Yorks, S. K. Miller, B. F. Taubman, G.
1594 Verver, H. Vömel, M. A. Avery, J. W. Hair, G. S. Diskin, E. V. Browell, J. M. Valverde-
1595 Canossa, T. L. Kucsera, C. A. Klich, D. L. Hlavka (2010), Convective and wave signatures in
1596 ozone profiles over the equatorial Americas: Views from TC4 (2007) and SHADOZ, *J.*
1597 *Geophys. Res.*, doi: 10.1029/2009JD012909, submitted to this special issue.

1598 Thornberry, T., K. D. Froyd, D. M. Murphy, D. S. Thomson, B. E. Anderson, K. L. Thornhill,
1599 and E. L. Winstead (2010), Persistence of organic carbon in heated aerosol residuals
1600 measured during TC4, *J. Geophys. Res.*, submitted to this special issue.

1601 Thuburn, J. and G. C. Craig (2002), On the temperature structure of the tropical substratosphere,
1602 *J. Geophys. Res.*, *107*(D2), 10.1029/2001JD000448.

1603 Tian, L., G. M. Heymsfield, A. J. Heymsfield, A. Bansemer, L. Li, C. Twohy, R. C. Srivastava
 1604 (2009), A study of cirrus ice particle size distributions using TC4 observations, *J. Atmos. Sci.*,
 1605 in press.

1606 Vömel, H., D. E. David, and K. Smith (2007a), Accuracy of tropospheric and stratospheric water
 1607 vapor measurements by the cryogenic frost point hygrometer: Instrumental details and
 1608 observations, *J. Geophys. Res.*, *112*, D08305, doi:10.1029/2006JD007224.

1609 Vömel, H., V. Yushkov, S. Khaykin, L. Korshunov, E. Kyrö and R. Kivi (2007b),
 1610 Intercomparisons of stratospheric water vapor sensors: FLASH-B and NOAA/CMDL Frost-
 1611 Point Hygrometer, *J. Atmos. Ocean. Tech.*, *24*, 941-952, doi:10.175/JTECH2007.1.

1612 Vömel, H., et al. (2002), Balloon-borne observations of water vapor and ozone in the tropical
 1613 upper troposphere and lower stratosphere, *J. Geophys. Res.*, 10.1029/2001JD000707.

1614 Wang Y.H., et al. (2001), Factors controlling tropospheric O₃, OH, NO_x and SO₂ over the
 1615 tropical Pacific during PEM-Tropics B, *J. Geophys. Res.*, *106*, 32733-32747.

1616 Wennberg P. O. et al. (1998), Hydrogen radicals, nitrogen radicals, and the production of O₃ in
 1617 the upper troposphere, *Science*, *279*, 49-53.

1618 Weisenstein, D.K., G. K. Yue, M. K. W. Ko, N. D. Sze, J. M. Rodriguez, C. J. Scott (1997), A
 1619 two-dimensional model of sulfur species and aerosols, *J. Geophys. Res.*, *102*, 13019-13035.

1620
 1621 **Figure captions**

1622 **Figure 1.** Early morning on 5 August, 2007 at the Juan Santamaria International Airport in Costa
 1623 Rica. From left to right NASA's DC-8, WB-57F, and ER-2 prepare for a flight. In the
 1624 background a large mesoscale convective complex in the Pacific Ocean near Costa Rica rises
 1625 into the Tropopause Transition Layer. The aircraft investigated this feature for several hours,
 1626 until it dissipated. Photo by Sean Davis.

1627
 1628 **Figure 2.** Schematic of troposphere-to-stratosphere transport pathways across the TTL.

1629
 1630 **Figure 3.** The NASA ER-2 and its instrument complement as flown in TC4.

1631
 1632 **Figure 4.** The NASA WB-57F and its instrument complement as flown in TC4.

1633
 1634 **Figure 5.** The NASA DC-8 showing the instruments used in TC4 and their placement on the
 1635 aircraft

1636
 1637 **Figure 6.** The University of Oklahoma SMART radar located at Juan Santamaria International
 1638 Airport in Costa Rica.

1639
 1640 **Figure 7.** The NASA polarization (NPOL) radar and the NATIVE trailer located in Las Tablas,
 1641 Panama.

1642
 1643 **Figure 8.** The ER-2 (blue) and DC-8 (red) flight tracks for 17 July, 2007 are superimposed on a
 1644 GOES retrieved optical depth map. Approximate take off and landing times are given for the
 1645 DC-8 and ER-2 in the top left corner. San Jose Costa Rica is marked with a yellow square.
 1646 The aircraft altitudes are given in the bottom left insert. The flight tracks are superimposed on
 1647 cloud optical depth retrieved from the GOES image whose time is given in the black bar at the
 1648 bottom of the figure. Note that optical depths above 100 are reported in the core of the mesoscale

1649 complex, while most of the aircraft sampling was in regions with optical depths in the range
1650 from 1 to 10.

1651 http://www-angler.larc.nasa.gov/tc4/fltrks/jul17/products/ALL_ALL.TAU.2007198.1645.gif

1652
1653 **Figure 9.** The ER-2 flight track for 19 July, 2007. Labels are explained in Figure 8. The flight
1654 track is superimposed on a visible image which composites GOES 10 and GOES 12 data.

1655 <http://www-angler.larc.nasa.gov/tc4/fltrks/jul19/ER2.SEG.GOESVIS.2007200.1515.gif>

1656
1657 **Figure 10.** The DC-8 flight track for 21 Jul, 2007. The flight track is on top of a visible
1658 wavelength GOES image. Labels are explained in Figure 8.

1659 <http://angler.larc.nasa.gov/tc4/fltrks/jul21/DC8.ALL.GOESVIS.2007202.1615.gif>

1660
1661 **Figure 11.** The ER-2 and DC-8 flight tracks for 22 July, 2007. Figure labels are explained in
1662 Figure 8. Also noted are overpass paths for TRMM (yellow), and for CALIPSO (blue). The
1663 background is a GOES 10+Goes 12 infrared brightness temperature image.

1664 http://www-angler.larc.nasa.gov/tc4/fltrks/jul22/ALL_ALL.GOESIR.2007203.1515.gif

1665
1666 **Figure 12.** The tracks of the DC-8 and ER-2 for 24 July, 2007. For an explanation of the keys
1667 see Figure 8. The flight tracks are superimposed on a GOES infrared brightness temperature
1668 image.

1669 http://www-angler.larc.nasa.gov/tc4/fltrks/jul24/ALL_ALL.GOESIR.2007205.1528.gif

1670
1671 **Figure 13.** The track of the ER-2 for 25 July, 2007. For an explanation of the keys see Figure 8.

1672 The GOES image has been processed to obtain the cloud optical depths. [http://www-](http://www-angler.larc.nasa.gov/tc4/fltrks/jul25/products/ER2.TAU.2007206.1615.gif)

1673 [angler.larc.nasa.gov/tc4/fltrks/jul25/products/ER2.TAU.2007206.1615.gif](http://www-angler.larc.nasa.gov/tc4/fltrks/jul25/products/ER2.TAU.2007206.1615.gif)

1674
1675 **Figure 14.** The DC-8 flight track for 28 July, 2007, superimposed on a GOES visible image. For
1676 an explanation of the keys see Figure 8.

1677 http://angler.larc.nasa.gov/tc4/fltrks/jul28/dc8_index.html

1678
1679 **Figure 15.** The DC-8 and ER-2 flight tracks for 29 July, 2007, superimposed on a GOES 10/12
1680 composite visible image. See Figure 8 for explanations of the other information on the figure.
1681 Note the yellow line is the TERRA overpass line, while the orange line is the
1682 CALIPSO/CloudSat track.

1683 http://angler.larc.nasa.gov/tc4/fltrks/jul29/allplane_index.htmhttp://angler.larc.nasa.gov/tc4/fltrks/jul29/allplane_index.html

1684
1685
1686 **Figure 16.** The flight tracks of the ER-2 and DC-8 on 31 July, 2007, superimposed on a GOES
1687 retrieval of ice water path. Figure 8 explains the keys in the figure.

1688 http://www-angler.larc.nasa.gov/tc4/fltrks/jul31/products/ALL_ALL.IWP.2007212.1615.gif

1689
1690 **Figure 17.** The convective complex seen from the DC-8 at the southern edge of the race tracks in
1691 Figure 16, where the sky was relatively clear. In most of the race track the DC-8 was flying
1692 relatively low in the anvil, where ice crystals were falling down from above. The ER-2 recorded
1693 the cloud tops near 15-16 km, well above the DC-8 ceiling of 12 km. Photo by Paul Wennberg

1694

1695 **Figure 18.** The DC-8, ER-2 and WB-57F flight tracks for 3 August, 2007 superimposed on a
1696 GOES infrared brightness temperature image. The white line is the CloudSat and CALIPSO
1697 overpass track. For an explanation of the keys see Figure 8.

1698 http://www-angler.larc.nasa.gov/tc4/fltrks/aug03/ALL_ALL.GOESIR.2007215.1428.gif

1699
1700 **Figure 19.** The flight tracks of the DC-8, ER-2 and WB-57F on 5 Aug. 2007 superimposed on a
1701 GOES infrared brightness temperature image. For an explanation of the keys see Figure 8.

1702 http://www-angler.larc.nasa.gov/tc4/fltrks/aug05/ALL_ALL.GOESIR.2007217.1558.gif

1703
1704 **Figure 20.** The flight tracks of the DC-8, the ER-2 and the WB-57F on 6 August, 2007,
1705 superimposed on a GOES 10+12 visible image. The yellow line is the Terra overpass track. For
1706 an explanation of the keys see Figure 8.

1707 http://angler.larc.nasa.gov/tc4/fltrks/aug06/allplane_index.html

1708
1709 **Figure 21.** A false color MODIS-Aster Airborne Simulator (MASTER) image of the Von
1710 Kármán vortex sampled by the DC-8 on August 6, 2007 just north of the Galapagos Islands
1711 (RGB = 2.1, 1.6, and 0.66 μm channels). The light blue color indicates relatively large cloud
1712 droplet sizes in these stratus clouds. The instrument's swath width (vertical dimension) is about
1713 37 km, while the length of the flight leg is about 90 km. Courtesy of Steven Platnick.

1714
1715 **Figure 22.** The flight tracks of the DC-8, ER-2 and WB-57F for 8 August, 2007 superimposed
1716 on a GOES infrared brightness temperature image. For an explanation of the keys see Figure 8.

1717 http://www-angler.larc.nasa.gov/tc4/fltrks/aug08/ALL_ALL.GOESIR.2007220.1528.gif

1718
1719
1720
1721

1721 **Table 1.** Major questions addressed by TC4

Scientific question

1. What mechanisms maintain the humidity of the stratosphere? What are the relative roles of large-scale transport and convective transport and how are these processes coupled?
 2. What are the physical mechanisms that control (and cause) long-term changes in the humidity of the upper troposphere in the tropics and subtropics?
 3. What controls the formation, maintenance and distribution of thin cirrus in the TTL, and what is the influence of thin cirrus on radiative heating and cooling rates, and on vertical transport?
 4. What are the chemical fates of short-lived compounds transported from the tropical boundary layer into the TTL? (i.e., what is the chemical boundary condition for the stratosphere?)
 5. What are the mechanisms that control ozone within and below the TTL? What is the chemical nature of the outflow from convective regions?
 6. How do convective intensity and aerosol properties affect cirrus anvil properties?
 7. How do cirrus anvils, and tropical cirrus in general, evolve over their life cycle? How do they impact the radiation budget and ultimately the circulation?
 8. How can space-based measurements of geophysical parameters, particularly those known to possess strong variations on small spatial scales (e.g., H₂O, cirrus), be validated in a meaningful fashion?
-

1722

1722

1723 **Table 2.** TC4 science flights

Date	DC-8	ER-2	WB-57	Comments
13 July	X			Transit to Costa Rica
14 July		X		Transit to Costa Rica
17 July	X	X		
19 July		X		DC-8 not flown due to flap actuator problem.
21 July	X			ER-2 not flown (some instruments down)
22 July	X	X		
24 July	X	X		Lightning strike on DC-8
25 July		X		DC-8 not flown due to lightning strike on DC-8 on previous flight.
28 July	X			ER-2 not flown (some instruments down)
29 July	X	X		
31 July	X	X		
3 August	X	X	X	Transit to Costa Rica, WB-57F
5 August	X	X	X	
6 August	X	X	X	
8 August	X	X	X	
9 August		X	X	Return home
10 August	X			Return home
13 August			X	Houston WB-57F science flight

1724

1725

1725
 1726
 1727

Table 3. Satellite instruments

Instrument	Satellite	Investigator	Institution	Measurements of relevance to TC4
OMI	Aura	P. Levelt	KNMI	SO ₂ ; aerosols
TES	Aura	R. Beer	JPL	Ozone
HIRDLS	Aura	J. Gille	NCAR	Temperature profiles
MLS	Aura		JPL	Cloud and water vapor
CALIOP	CALIPSO	D. M. Winker	NASA Langley	aerosol extinction
Cloud Profiling Radar	CloudSat	G. Stephens	Colorado State, JPL	radar backscatter
MODIS	Terra	V. Salomonson	NASA Goddard	Cloud properties
MODIS	Aqua	V. Salomonson	NASA Goddard	Cloud properties
Precipitation radar, Microwave imager	TRMM	S. Braun	NASA Goddard	Rainfall rates
Visible and infrared imager	GOES 10/12	P. Minnis	NASA Langley	Cloud properties

1728
 1729

Table 4. ER-2 Instruments

Instrument	Name	PI	Products
CPL	Cloud Physics Lidar (532, 1064 nm)	Matthew McGill NASA GSFC	Cloud/aerosol detection and layer information (top/base altitudes, extinction)
CRS	Cloud Radar System (94 GHz)	Gerry Heymsfield, NASA GSFC	Radar reflectivity, Doppler velocities, cloud layer water content
EDOP	ER-2 Doppler Radar (X band)	Gerry Heymsfield, NASA GSFC	Radar reflectivity, Doppler velocities, precipitation
AMPR	Advanced Microwave Precipitation Radiometer (10.7, 19.4, 37, 89 GHz)	Robbie Hood, NASA MSFC	Precipitation Index
MAS/MASTER	MODIS, MODIS-ASTER (starting July 29) Airborne Simulator (VIS/NIR/SWIR/IR spectrometer)	Michael King, NASA GSFC	Cloud properties, ice and water (cloud top, optical thickness, effective particle size, WP)
CoSSIR	Conical Scanning Sub-mm Wave Imaging Radiometer (183 - 874 GHz)	James Wang, NASA GSFC	IWP, ice cloud median mass particle diameter, moisture profiles
S-HIS	Scanning High Resolution Interferometer Sounder (3-18 μm)	Hank Revercomb Univ. Wisconsin	Temperature/ moisture profiles, cirrus cloud properties (top pressure, optical thickness, effective particle size), IWP
BB IR	Broad Band Radiometer (4 - 42 μm)	Anthony Bucholtz, NRL	IR radiative fluxes and layer heating rate (w/similar instrument on DC-8)
SSFR	Solar Spectral Flux Radiometer (VIS-SWIR)	Peter Pilewskie, Colorado Univ.	Solar spectral fluxes and layer heating rate (also on DC-8), ice cloud properties
MTP	Microwave Temperature Profiler	M.J. Mahoney, NASA JPL	Temperature vs Pressure Altitude near aircraft, Molecular number density vs Pressure Altitude
MVIS	Video Camera	Jeff Myers, Ames	

1732
1733

Table 5a. WB-57F In Situ water and Particle Instruments

WB-57 Instrument Summary			
Instrument	Name	PI	Products
CLH	Closed-Path Laser Hygrometer	Linnea Avallone, U. Colorado	Ice Water Content
Frostpoint (FP)	Frostpoint Hygrometer	David W. Fahey, NOAA	Water vapor mixing ratio
H2Ov	Water Vapor	Elliot Weinstock, Harvard	Water vapor mixing ratio
HOxotope	HOx/Isotope	Tom Hanisco, Harvard	Total water (vapor + condensed), H ₂ O and HDO
ICOS	Integrated Cavity Spectrometer	Tom Hanisco, Harvard	Water vapor isotopologue (H ₂ ¹⁶ O, H ₂ ¹⁷ O, H ₂ ¹⁸ O, HDO) and CH ₄ mixing ratio
JLH	JPL Laser Hygrometer	Robert Herman, NASA JPL	H ₂ O vol. mixing ratio,
2DS	2D-S Probe	Paul Lawson, SPEC Inc.	Cloud Particles images, Particle size distributions
CAPS	Cloud, Aerosol & Precipitation Spectrometer	Bruce Gandrud, Droplet Measurements	Concentration, Ice Water Content, Surface Area Extinction Coefficient
CDP	Cloud Droplet Probe	Bruce Gandrud, Droplet Measurements	Concentration, Ice Water Content, Surface Area, Extinction Coefficient, Median Volume Diameter
CEM	Transmissometer	Paul Lawson, SPEC Inc.	Cloud Extinction
CPI	Cloud Particle Imager	Bruce Gandrud, Droplet Measurements	Cloud Particles images, Particle size distributions, Particle Concentration, Cloud Extinction, Ice Water Content
CSI	Cloud Spectrometer Impactor	Paul Lawson, SPEC Inc.	Condensed (ice plus liquid) water content
FCAS	Focused Cavity Aerosol Spectrometer	J. C. Wilson, Denver University	Number of Particles/mg air in 28 size bins from ~90 to ~1300 nm
NMASS	Nuclei Mode Aerosol Size Spectrometer	J. C. Wilson, Denver University	Number of Particles/mg air larger than 4 nm, 8nm, 16nm, 32 nm, 50 nm.
SP2	Single Particle Soot Photometer	Ru-Shan Gao, NOAA	Black Carbon

Table 5b. WB-57F Trace Gas, Atmospheric State and Remote Sensing Instruments

Trace Gases			
Argus	Diode Laser Spectrometer	Max Loewenstein, NASA Ames	CO, CH ₄ , N ₂ O
NO/NO _y	Nitric Oxide/NO _y Chemiluminescence	Andy Weinheimer, NCAR	NO and NO _y , NO, NO ₂ , NO _y
O ₃	Ozone	David W. Fahey, NOAA	O ₃ mixing ratio
PANTHER	Gas Chromatograph	James W. Elkins, NOAA	PAN, CO, H ₂ , Methane, N ₂ O, SF ₆ , CFC-11, CFC-12, CFC replacement compounds (HCFC-22, -141b,-142b) and hydrofluorocarbons, (HFC-134a), halon 1211, methyl halides (methyl chloride (CH ₃ Cl), methyl bromide, (CH ₃ Br), methyl iodide (CH ₃ I), sulfur dioxide (SO ₂) and carbon sulfide (COS).
CO ₂	Harvard CO ₂	Bruce Daube, Harvard University	CO ₂
UAS O ₃	Ozone	Ru-Shan Gao, NOAA	O ₃ mixing ratio
WAS	Whole Air Sampler	Elliot Atlas, University of Miami	Numerous trace gases
MMS	Pressure Transducer and Temperature Probe	Paul Bui, NASA ARC	Pressure, temperature, 3D winds
P/T	Pressure and Temperature	David W. Fahey, NOAA	Pressure, Temperature
CAFS	Actinic Flux Spectrometer	Rick Shetter, NCAR	Actinic Flux
ACAM	Digital Camera	Scott Janz, NASA GSFC	Forward scene

1735 **Table 6.** DC-8 Instruments

Instrument	Name	PI	Products
DLH	Open Path TDL	Glen Diskin, NASA LaRC	H ₂ O
2D-S, CPI	Cloud Probes	Paul Lawson, SPEC Inc.	Cloud particle size distribution and type (habit)
LARGE	Aerosol Spectrometers	Bruce Anderson, NASA LaRC	Particle size distribution, optical properties, CCN
PALMS	Particle Composition Mass Spectrometer	Dan Murphy, NOAA	Particle composition
CAPS, PIP CVI	Cloud Probes Counterflow Virtual Impactor	Andy Heymsfield, NCAR Cynthia Twohy, Oregon State	Cloud particle size, images Cloud water content
CIMS	Chemical Ion Mass Spectrometer	John Crouse, Caltech	Acids and organic peroxides, SO ₂
DACOM	TDL (DACOM)	Glen Diskin, NASA LaRC	CO, CH ₄ , N ₂ O
FAST OZ	Chemiluminescence Ozone Probe	Melody Avery, NASA LaRC	Ozone mixing ratio
MACDON- NA	IR gas analyzer	Stephanie Vay, NASA LaRC	CO ₂
SAGA	Mist Chamber	Jack Dibb, U. New Hampshire	NO ₃ ⁻ , SO ₄ ⁻ , aerosol composition
NO	Chemiluminescence Nitric Oxide	Ron Cohen, U. C., Berkley	NO
TD-LIF	Tunable Diode Laser	Ron Cohen, U. C., Berkley	NO ₂ , Alkyl nitrates, PAN
WAS Dropsondes	Whole Air Sampler Atmospheric Probe	Don Blake, U. C., Irvine Errol Korn, NCAR	Many trace gases Temperature, pressure, winds, relative humidity
MMS	Pressure and Temperature Probe	Paul Bui, NASA ARC	Pressure, temperature, winds
APR-2 LASE	Precipitation Radar IR Lidar	Eric Smith, NASA MSFC Ed Browell, NASA LaRC	Reflectivity, precipitation Water vapor, aerosol and cloud heights, aerosol type
DIAL	UV Lidar	Ed Browell, NASA LaRC	Ozone, aerosol and cloud heights, aerosol type
BB IR	Broadband Radiometer	Anthony Bucholtz NRL	IR radiative fluxes and layer heating rate
CAFS SSFR	UV-Vis Actinic Flux Solar Spectral Flux Radiometer	Rick Shetter, NCAR Peter Pilewskie, U.	Ozone zenith column Solar spectral fluxes and heating rate

DC-8 CAM Video

Rick Shetter, U. N.
Dakota

Nadir and forward video

1736

1736
1737

Table 7. Ground based instruments and balloons

Instrument	PI	Period of operation	Location	Products
Ticosonde	Henry Selkirk, Bay Area Environmental Research Institute	6/16/07- 8/15/07	Juan Santamaria International Airport, Alajuela, Costa Rica	Geopotential height, pressure, temperature, relative humidity, GPS winds, lat and long @ 0.5 Hz
CFH-ozone sondes	Holger Vömel, University of Colorado	7/1/07- 8/12/07	San Cristobal, Galapagos/ Juan Santamaria Airport, Costa Rica	Ozone and water vapor plus temperature, pressure and GPS winds @ ~1.4 Hz
NATIVE	Anne Thompson, Pennsylvania State University		Las Tablas, Panama	Temperature versus pressure, ozone, water vapor, winds
SMART	Michael Biggerstaff		Juan Santamaria airport, San Jose	Weather radar
NPOL	John Gerlach NASA Goddard Space Flight Center		Las Tablas, Panama	Polarization radar
NATIVE	Anne Thompson		Las Tablas, Panama	Ozone, NO/NO _y , SO ₂ , CO, lidar, sunphotometer, UV radiometer Aerosol size distribution

1738
1739
1740



Figure 1. Early morning on 5 August, 2007 at the Juan Santamaria International Airport in Costa Rica. From left to right NASA's DC-8, WB-57f, and ER-2 prepare for a flight. In the background a large mesoscale convective complex in the Pacific Ocean near Costa Rica rises into the Tropopause Transition Layer. The aircraft investigated this feature for several hours, until it dissipated. Photo by Sean Davis.

1741
1742
1743
1744
1745
1746
1747
1748
1749
1750
1751
1752

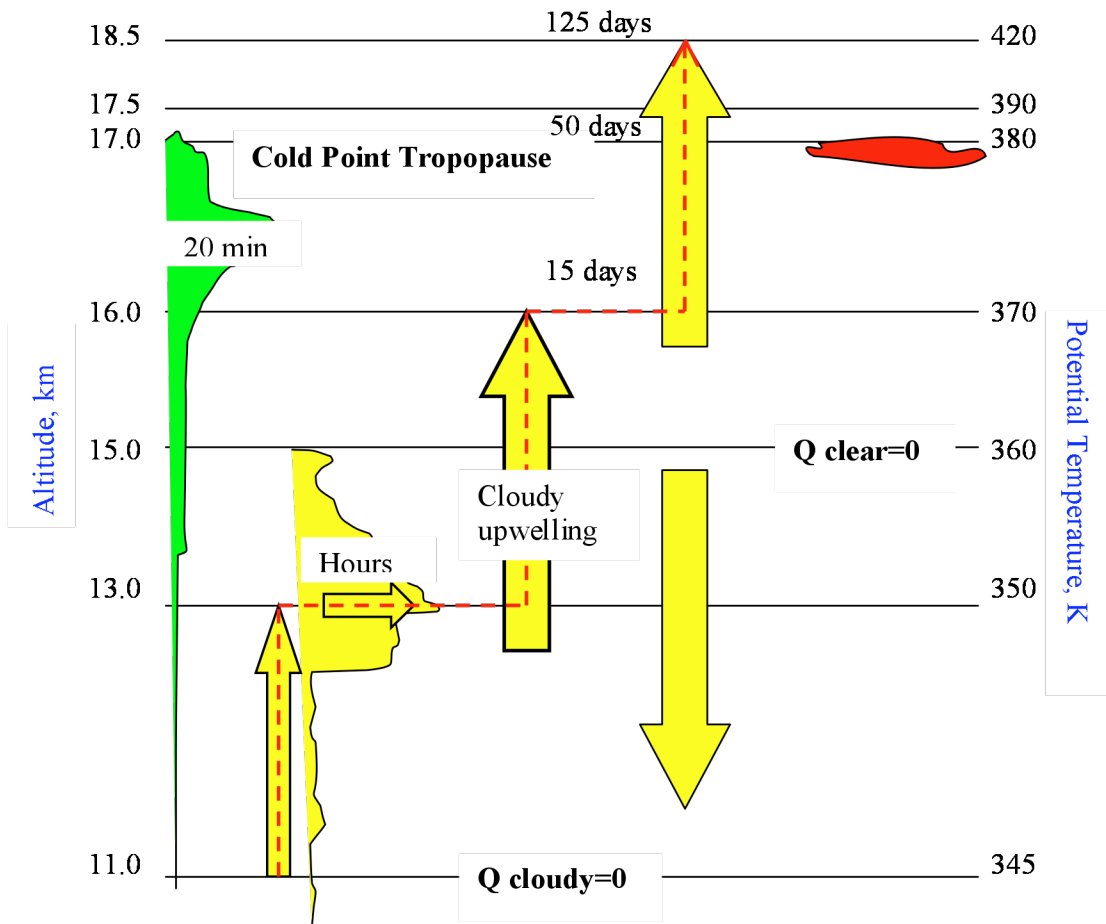
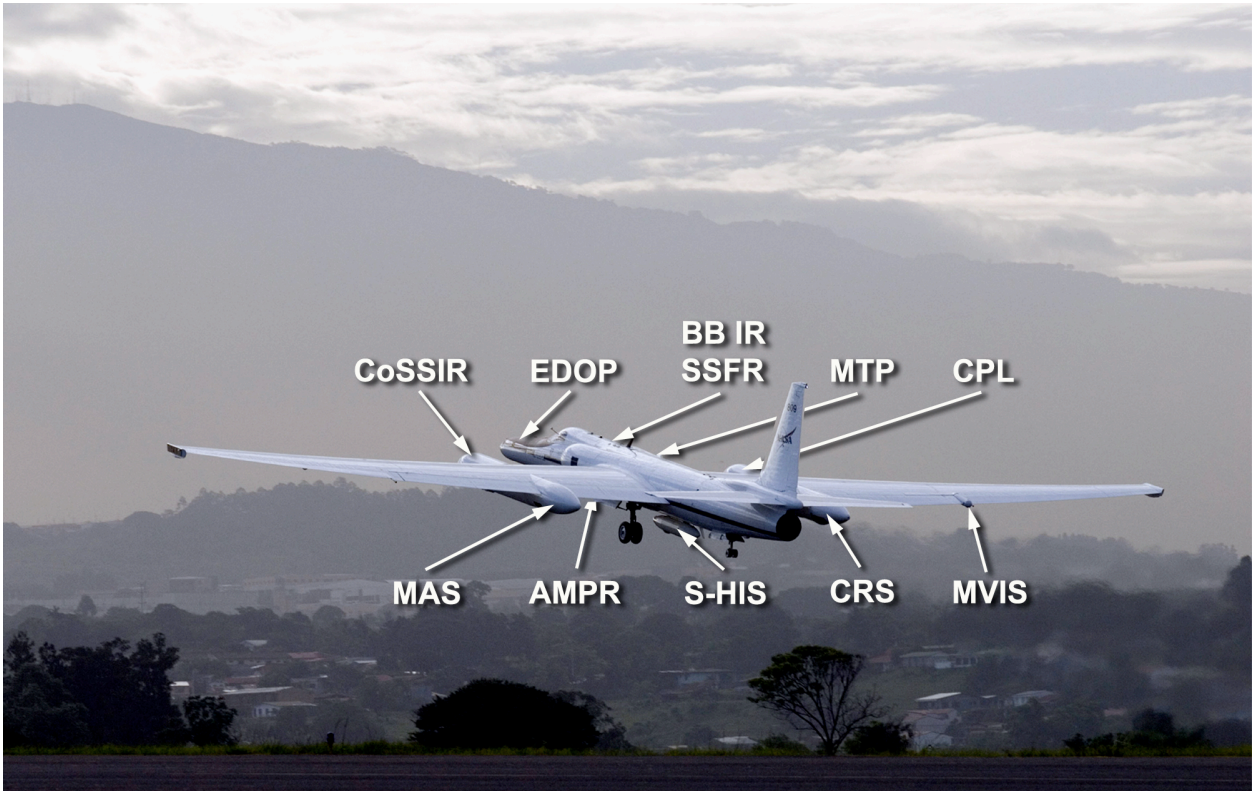


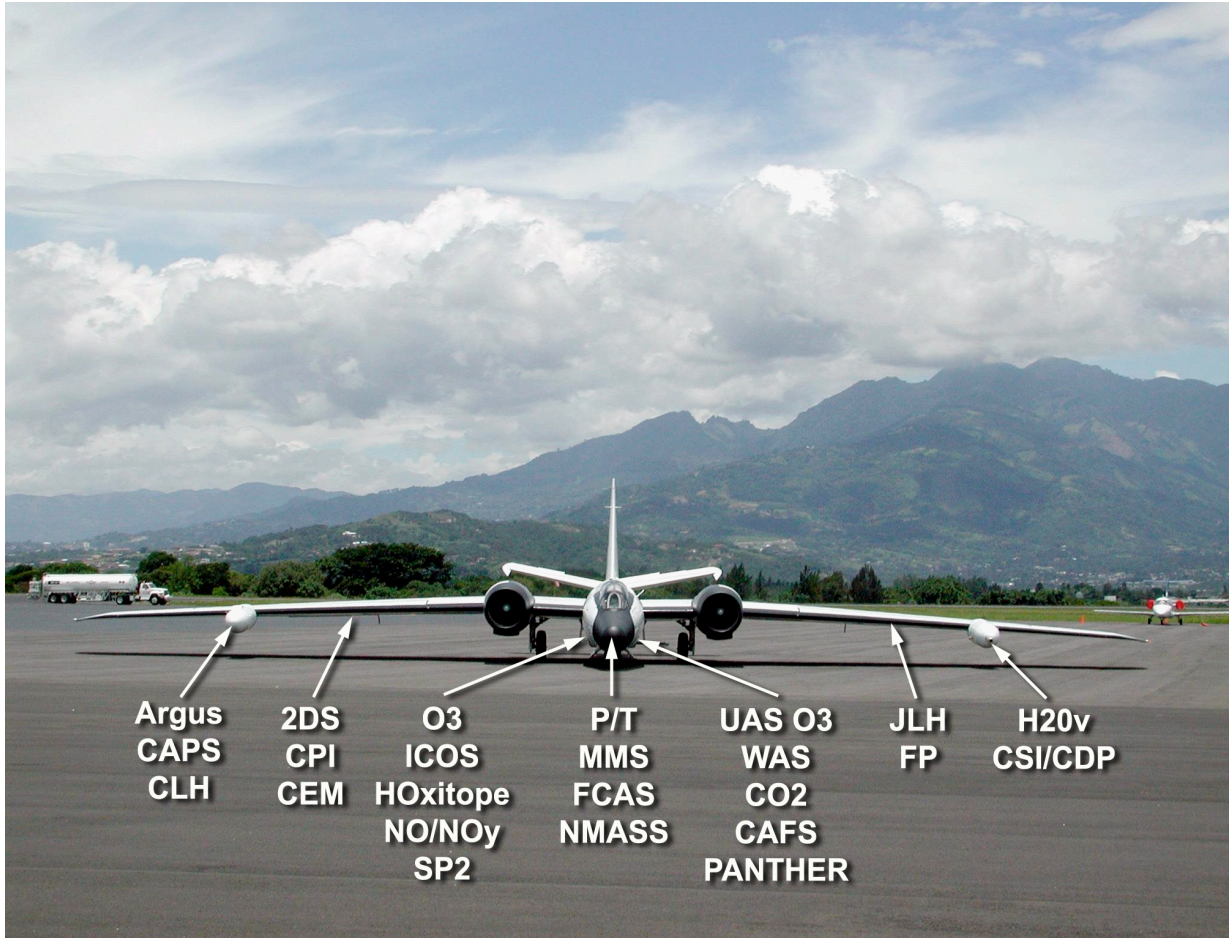
Figure 2. Schematic of three views of troposphere-to-stratosphere transport pathways across the TTL.

1752
1753
1754
1755



1779
1781
1783
1785
1787
1789
1791
1792
1793

Figure 3. The NASA ER-2 and its instrument complement as flown in TC4.



1820
1822
1824

Figure 4. The NASA WB-57f and its instrument compliment as flown in TC4.



1825
1826
1827
1828

1830

Figure 5. The NASA DC-8 showing the instruments used in TC4 and their placement on the aircraft.

1838

1839
1840



1869

Figure 6. The University of Oklahoma SMART radar near Juan Santamaria airport in Costa Rica.



Figure 7. The NASA polarization (NPOL) radar and the NATIVE trailer located in Las Tablas, Panama.

1870
1871
1872
1873

1873
1874
1875

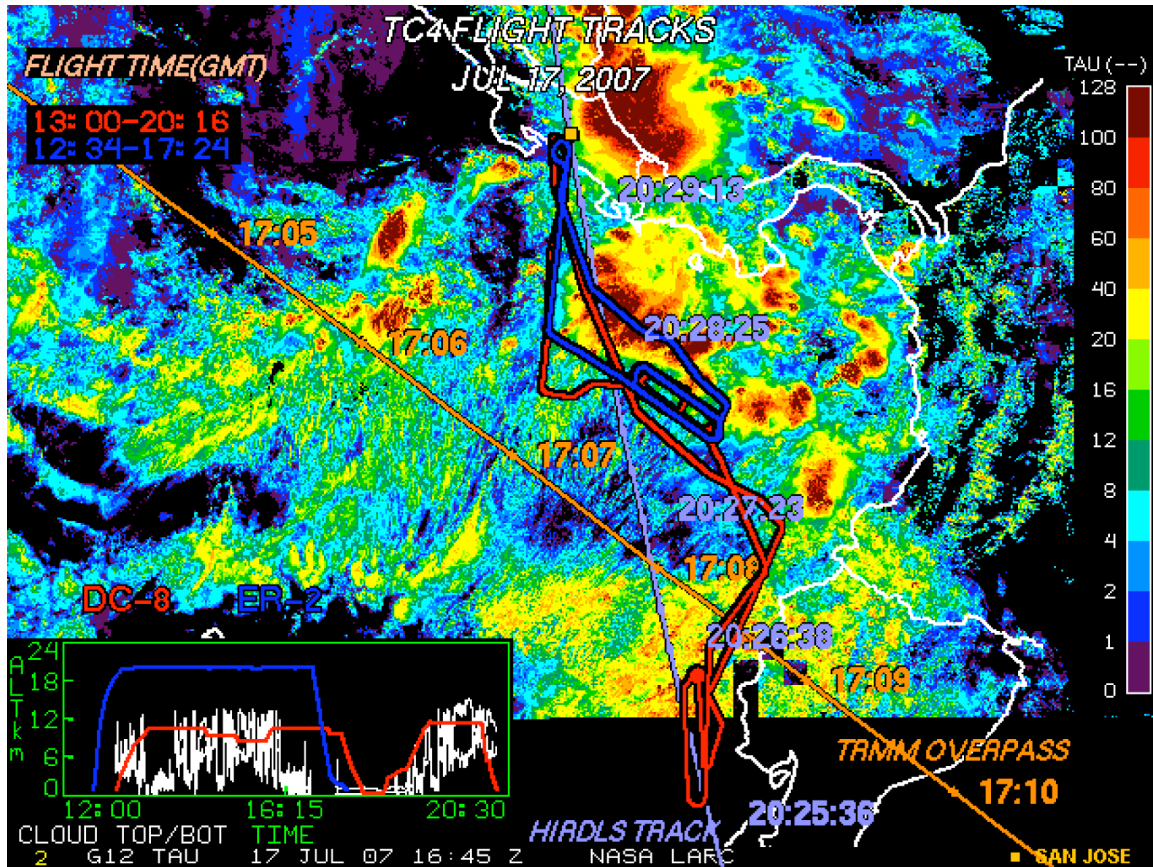


Figure 8. The ER-2 (blue) and DC-8 (red) flight tracks for 17 July, 2007 are superimposed on a GOES retrieved optical depth map. Approximate take off and landing times are given for the DC-8 and ER-2 in the top left corner. San Jose Costa Rica is marked with a yellow square. The aircraft altitudes are given in the bottom left insert. The flight tracks are superimposed on cloud optical depth retrieved from the GOES image whose time is given in the black bar at the bottom of the figure. Note that optical depths above 100 are reported in the core of the mesoscale complex, while most of the aircraft sampling was in regions with optical depths in the range from 1 to 10. The locations and times of a TRMM overpass and a HIRDLS overpass are also shown.
http://www-angler.larc.nasa.gov/tc4/flttrks/jul17/products/ALL_ALL.TAU.2007198.1645.gif

1875
1876
1877
1878

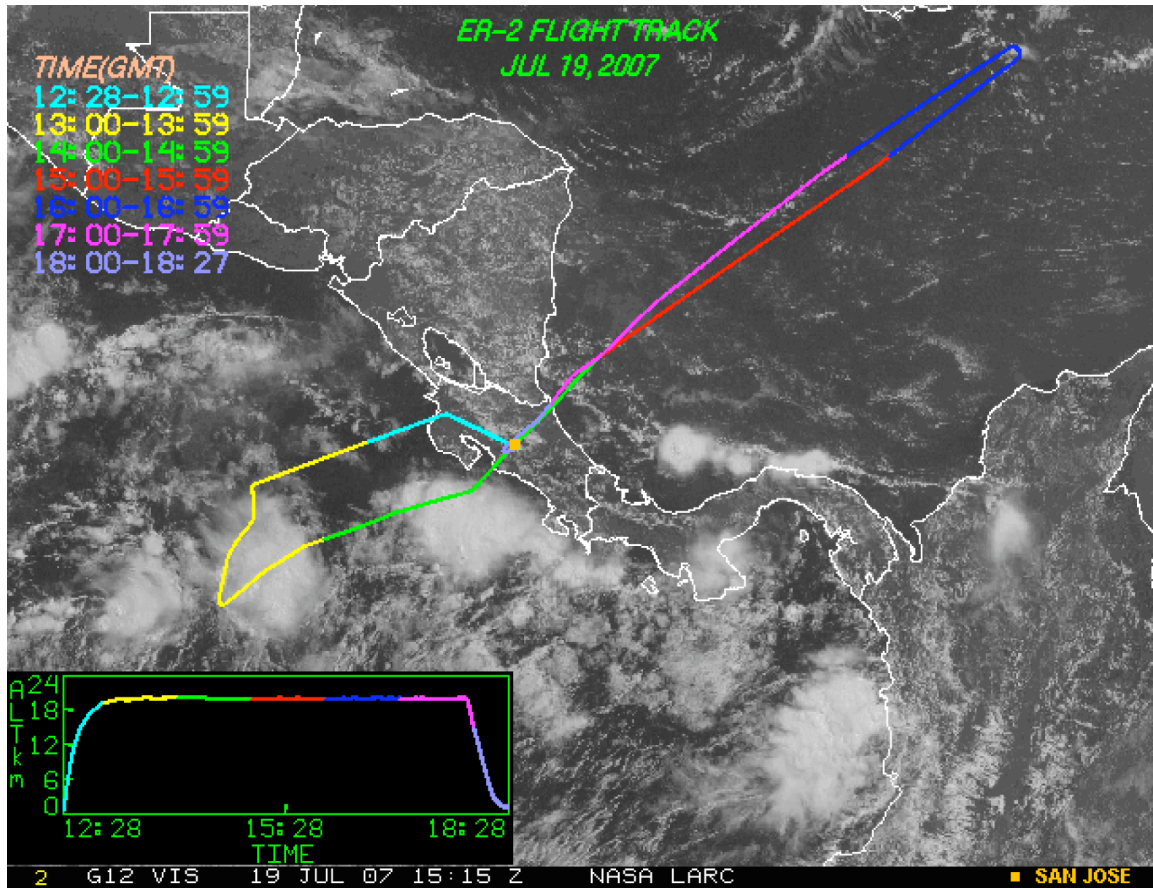


Figure 9. The ER-2 flight track for 19 July, 2007. Labels are explained in Figure 8. The flight track is superimposed on a visible image which composites GOES 10 and GOES 12 data.

<http://www-angler.larc.nasa.gov/tc4/flttrks/jul19/ER2.SEG.GOESVIS.2007200.1515.gif>

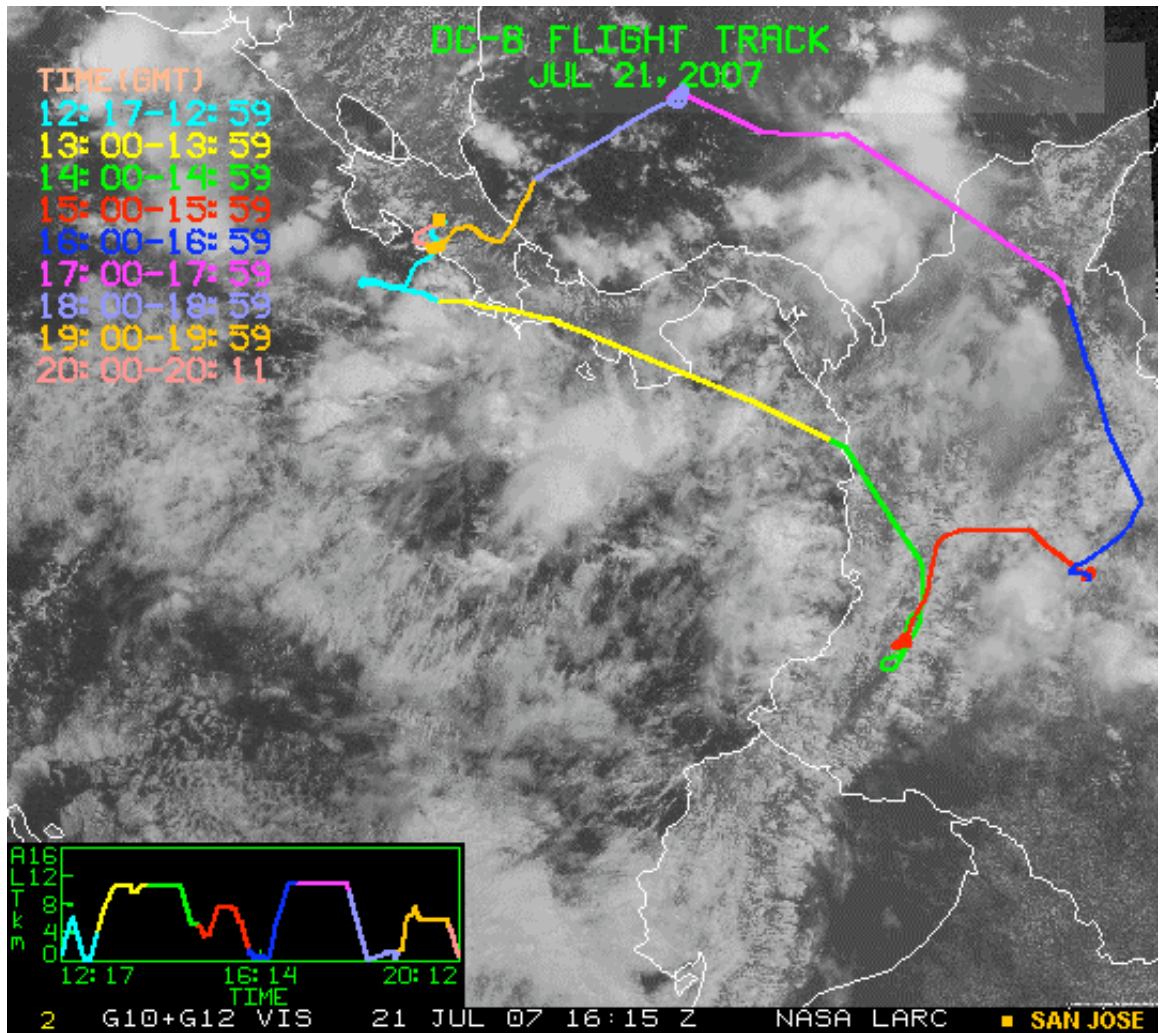


Figure 10. The DC-8 flight track for 21 July, 2007. The flight track is on top of a visible wavelength GOES image. Labels are explained in Figure 8. <http://angler.larc.nasa.gov/tc4/fltrks/jul21/DC8.ALL.GOESVIS.2007202.1615.gif>

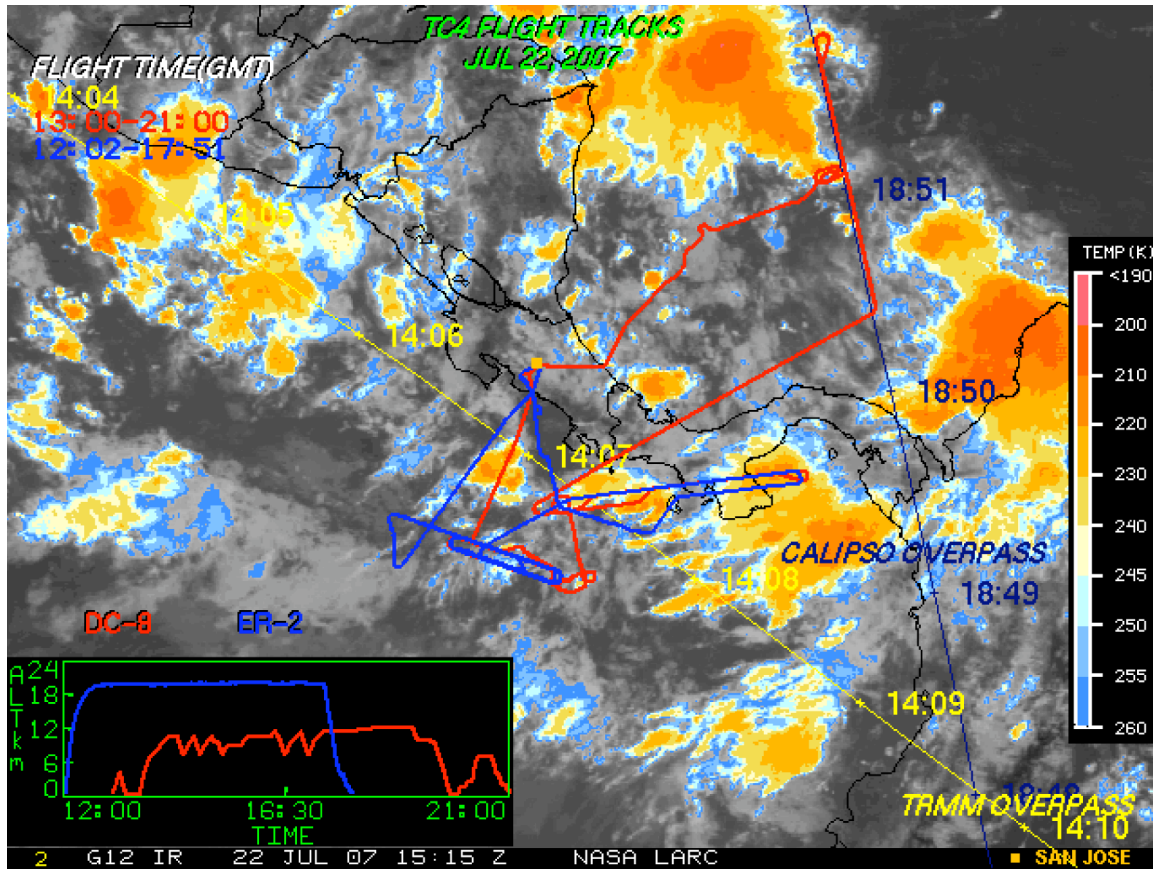


Figure 11. The ER-2 and DC-8 flight tracks for 22 July, 2007. Figure labels are explained in Figure 8. Also noted are overpass paths for TRMM (yellow), and for CALIPSO (blue). The background is a GOES 10+Goes 12 infrared brightness temperature image.

http://www-angler.larc.nasa.gov/tc4/fltrks/jul22/ALL_ALL.GOESIR.2007203.1515.gif

1884
1885
1886
1887
1888

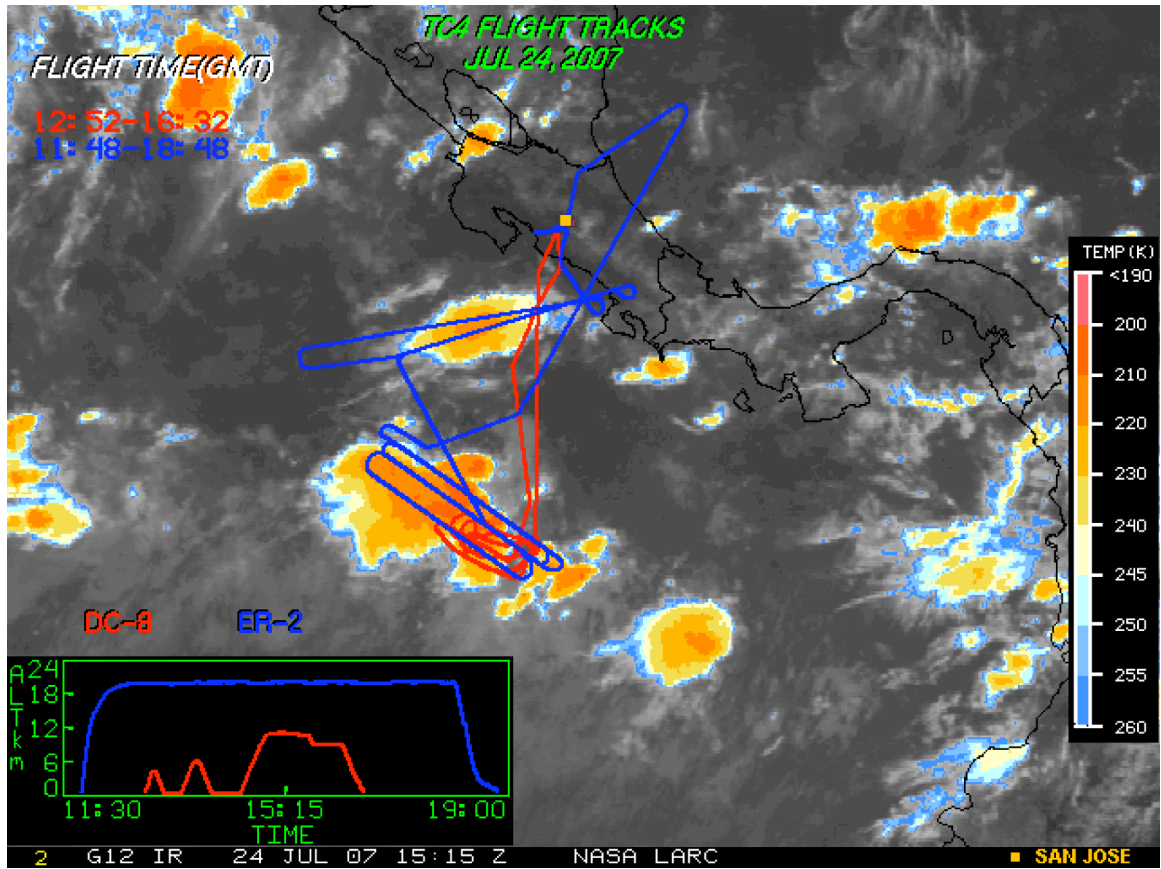


Figure 12. The tracks of the DC-8 and ER-2 for 24 July, 2007. For an explanation of the keys see Figure 8. The flight tracks are superimposed on a GOES infrared brightness temperature image.

http://www-angler.larc.nasa.gov/tc4/fltrks/jul24/ALL_ALL.GOESIR.2007205.1528.gif

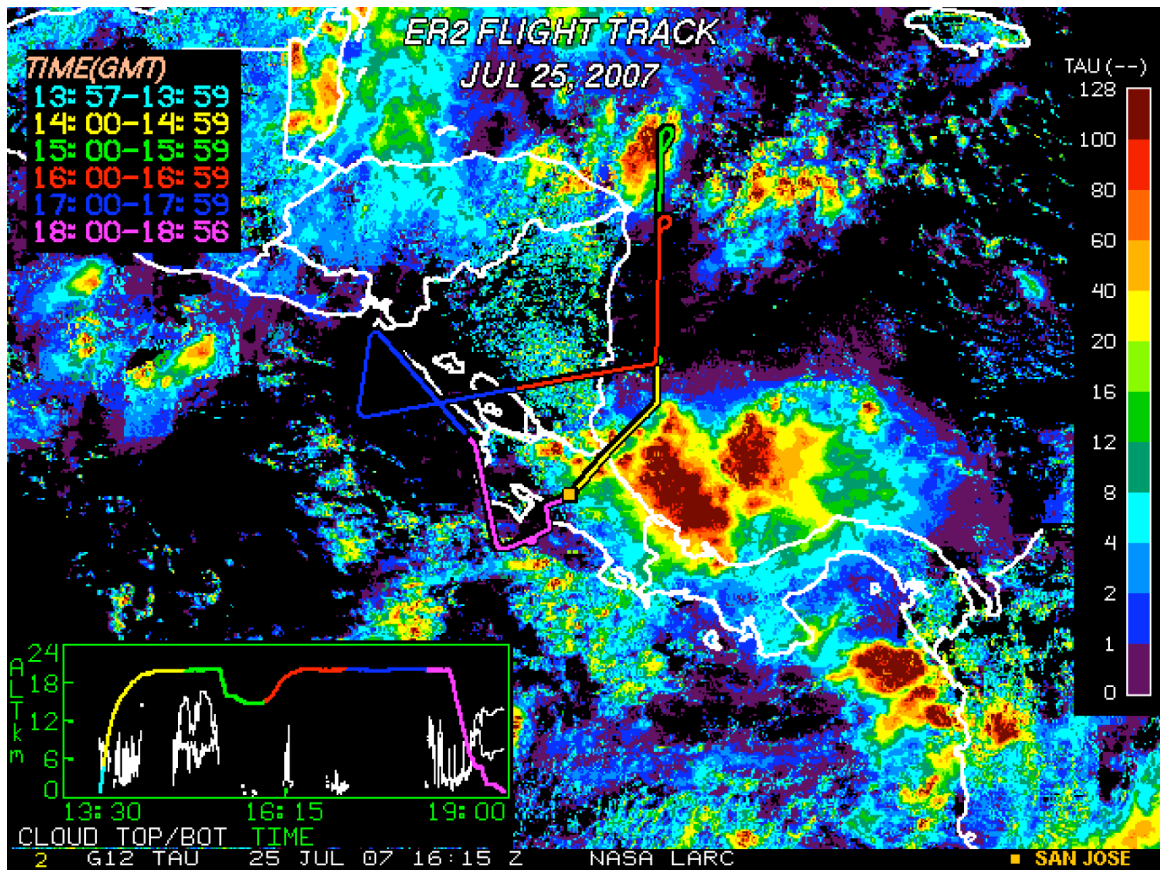


Figure 13. The track of the ER-2 for 25 July, 2007. For an explanation of the keys see Figure 8. The GOES image has been processed to obtain the cloud optical depths.
<http://www-angler.larc.nasa.gov/tc4/flttrks/jul25/products/ER2.TAU.2007206.1615.gif>

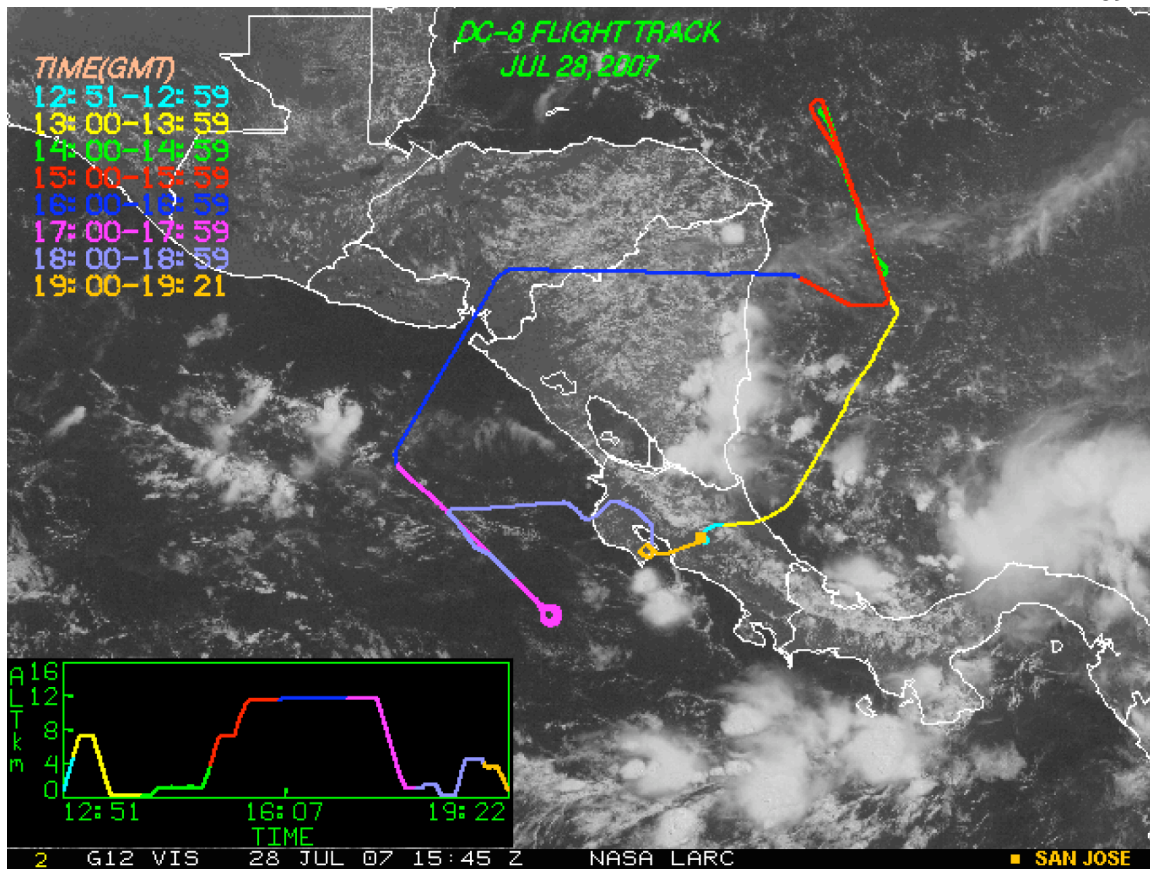


Figure 14. The DC-8 flight track for 28 July, 2007, superimposed on a GOES visible image. For an explanation of the keys see Figure 8.
http://angler.larc.nasa.gov/tc4/fltrks/jul28/dc8_index.html

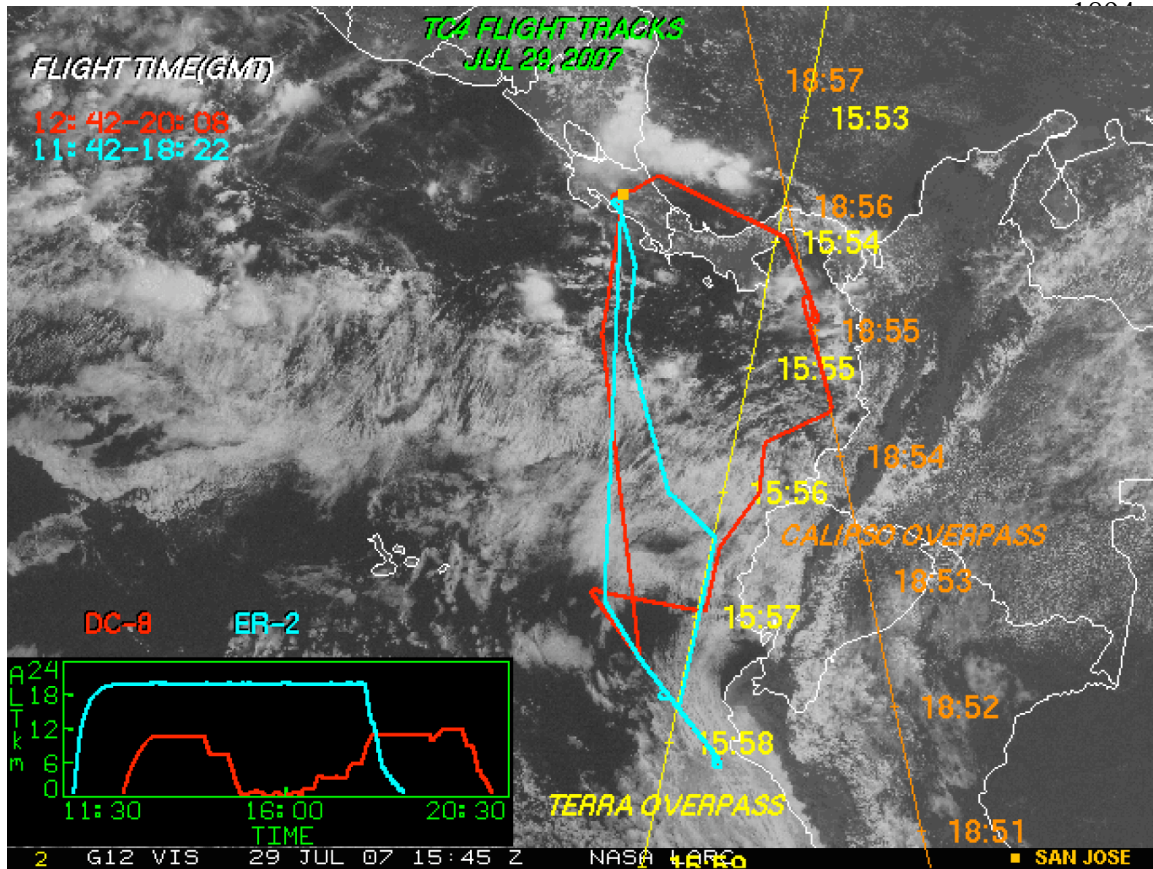


Figure 15. The DC-8 and ER-2 flight tracks for 29 July, 2007, superimposed on a GOES 10/12 composite visible image. See Figure 8 for explanations of the other information on the figure. Note the yellow line is the TERRA overpass line, while the orange line is the Calipso/CloudSat track.
http://angler.larc.nasa.gov/tc4/flttrks/jul29/allplane_index.html

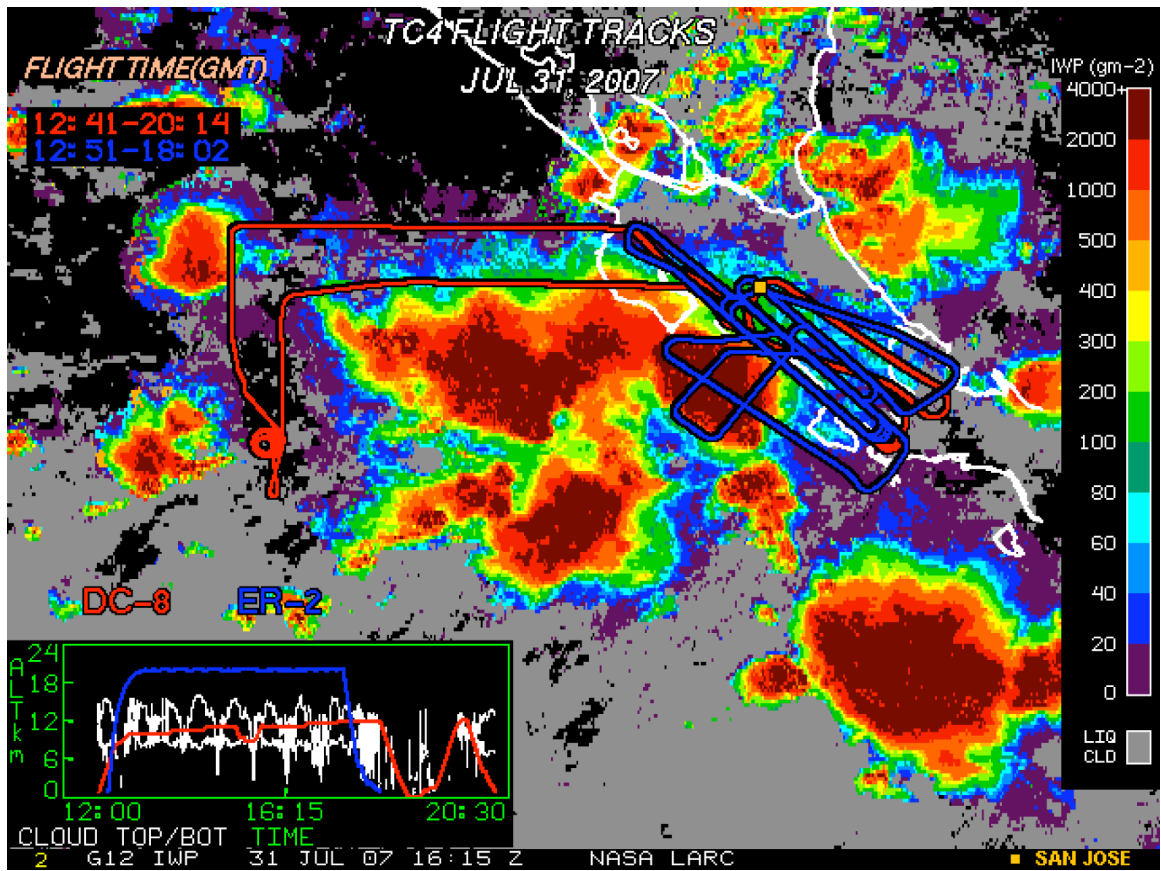


Figure 16. The flight tracks of the ER-2 and DC-8 on 31 July, 2007, superimposed on a GOES retrieval of ice water path. Figure 8 explains the keys in the figure.
http://www-angler.larc.nasa.gov/tc4/fltrks/jul31/products/ALL_ALL.IWP.2007212.1615.gif

1897
1898
1900
1902
1904



Figure 17. The convective complex seen from the DC-8 at the southern edge of the racetracks in Figure 16, where the sky was relatively clear. In most of the racetrack the DC-8 was flying relatively low in the anvil, where ice crystals were falling from above. The ER-2 recorded the cloud tops near 15-16 km, well above the DC-8 ceiling of 12 km. Photo by Paul Wennberg.

1905

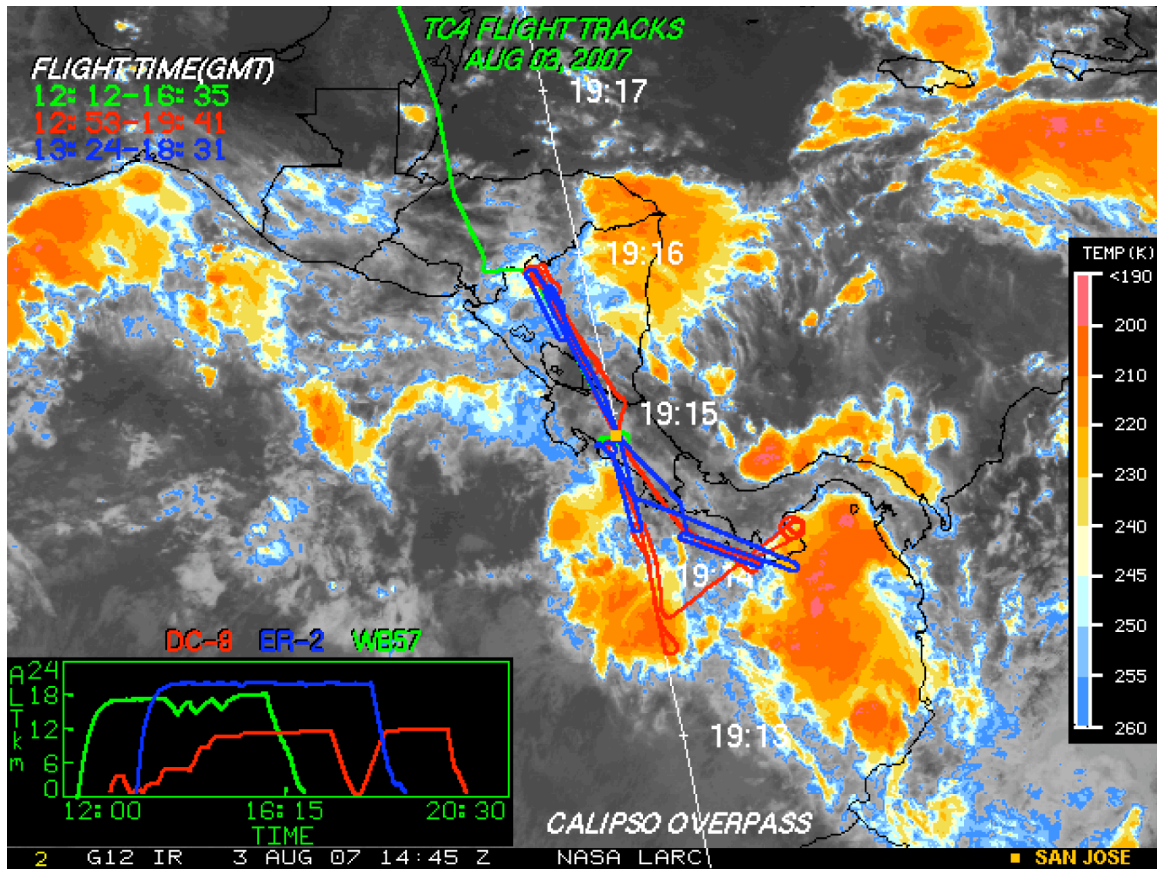


Figure 18. The DC-8, ER-2 and WB-57F flight tracks for 3 August, 2007 superimposed on a GOES infrared brightness temperature image. The white line is the CloudSat and Calipso overpass track. For an explanation of the keys see Figure 8.

http://www-angler.larc.nasa.gov/tc4/fltrks/aug03/ALL_ALL.GOESIR.2007215.1428.gif

1906

1907

1908

1909

1909
1910
1911
1912
1913

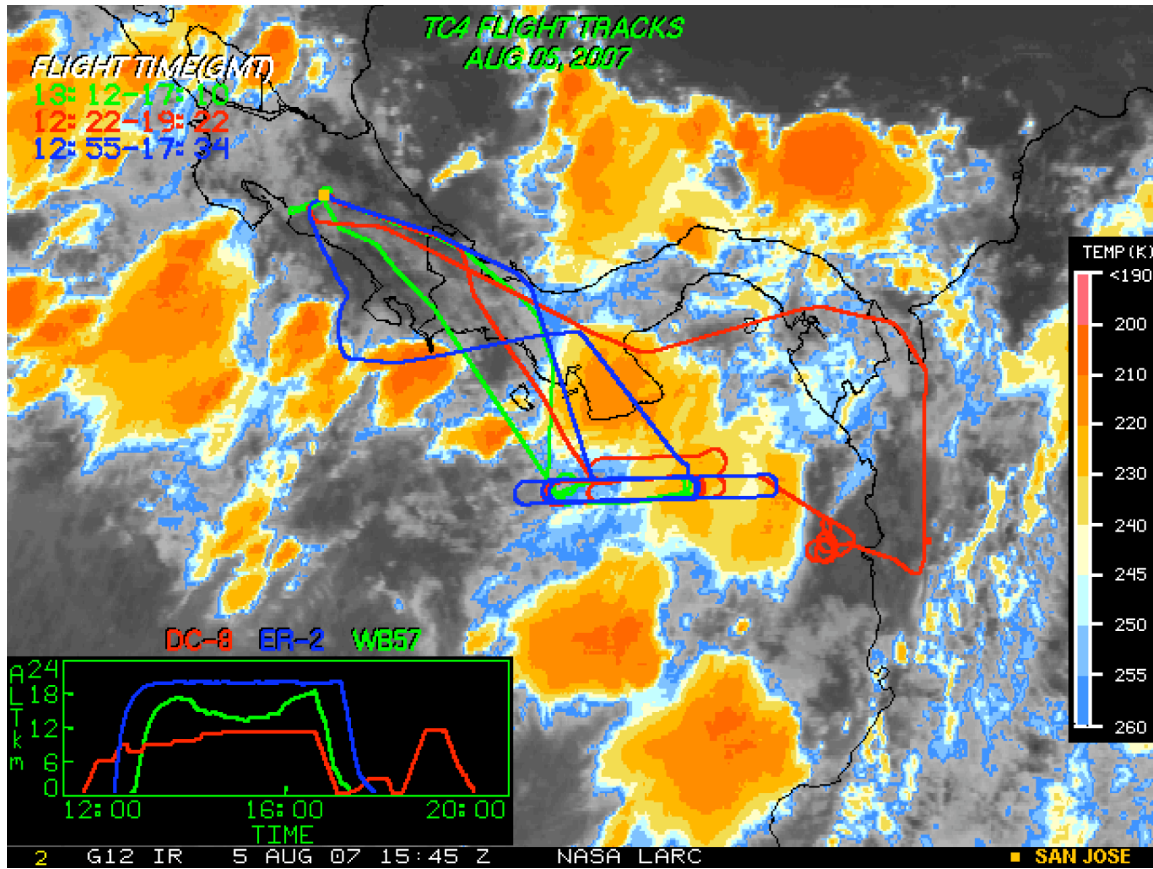


Figure 19. The flight tracks of the DC-8, ER-2 and WB-57F on 5 August 2007 superimposed on a GOES infrared brightness temperature image. For an explanation of the keys see Figure 8.

http://www-angler.larc.nasa.gov/tc4/flttrks/aug05/ALL_ALL.GOESIR.2007217.1558.gif

1913
1914
1915
1916

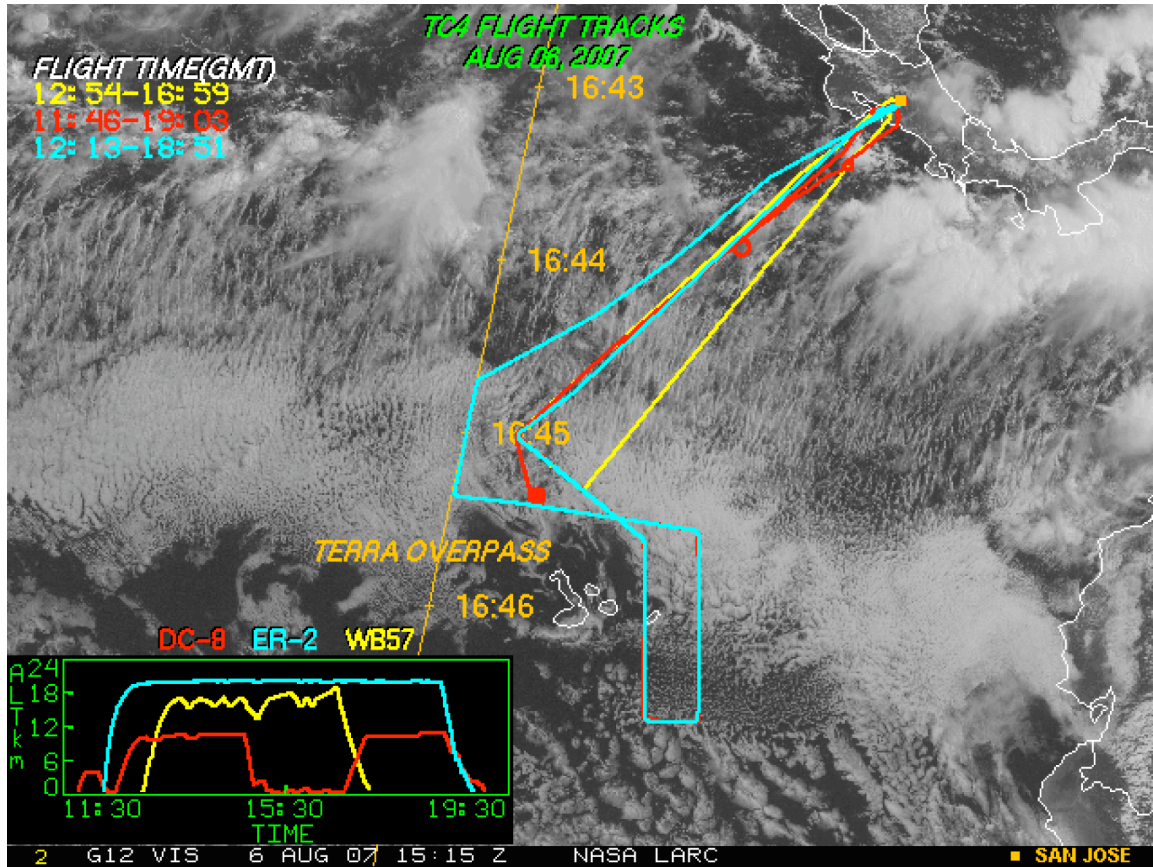
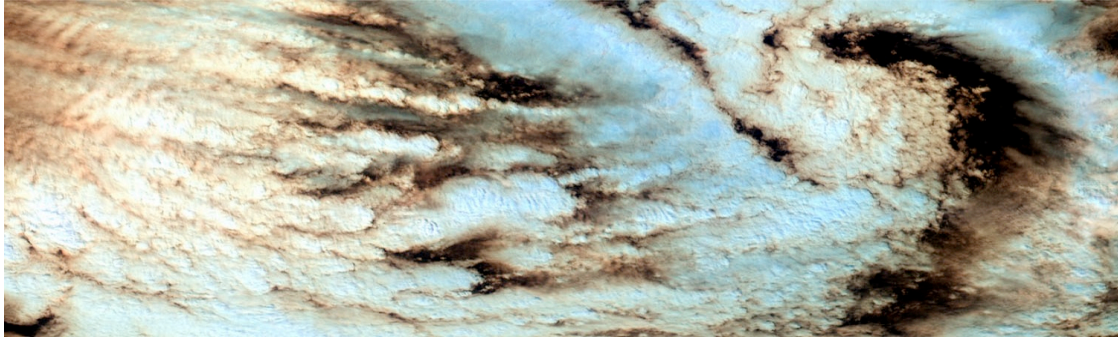


Figure 20. The flight tracks of the DC-8, the ER-2 and the WB-57F on 6 August, 2007, superimposed on a GOES 10+12 visible image. The yellow line is the Terra overpass track. For an explanation of the keys see Figure 8.
http://angler.larc.nasa.gov/tc4/fltrks/aug06/allplane_index.html



1916
1917
1918
1919
1920
1921

Figure 21. A false color MODIS-Aster Airborne Simulator (MASTER) image of the Von Karman vortex sampled by the DC-8 on August 6, 2007 just north of the Galapagos Islands (RGB = 2.1, 1.6, and 0.66 μm channels). The light blue color indicates relatively large cloud droplet sizes in these stratus clouds. The instrument's swath width (vertical dimension) is about 37 km, while the length of the flight leg is about 90 km. Courtesy of Steven Platnick.

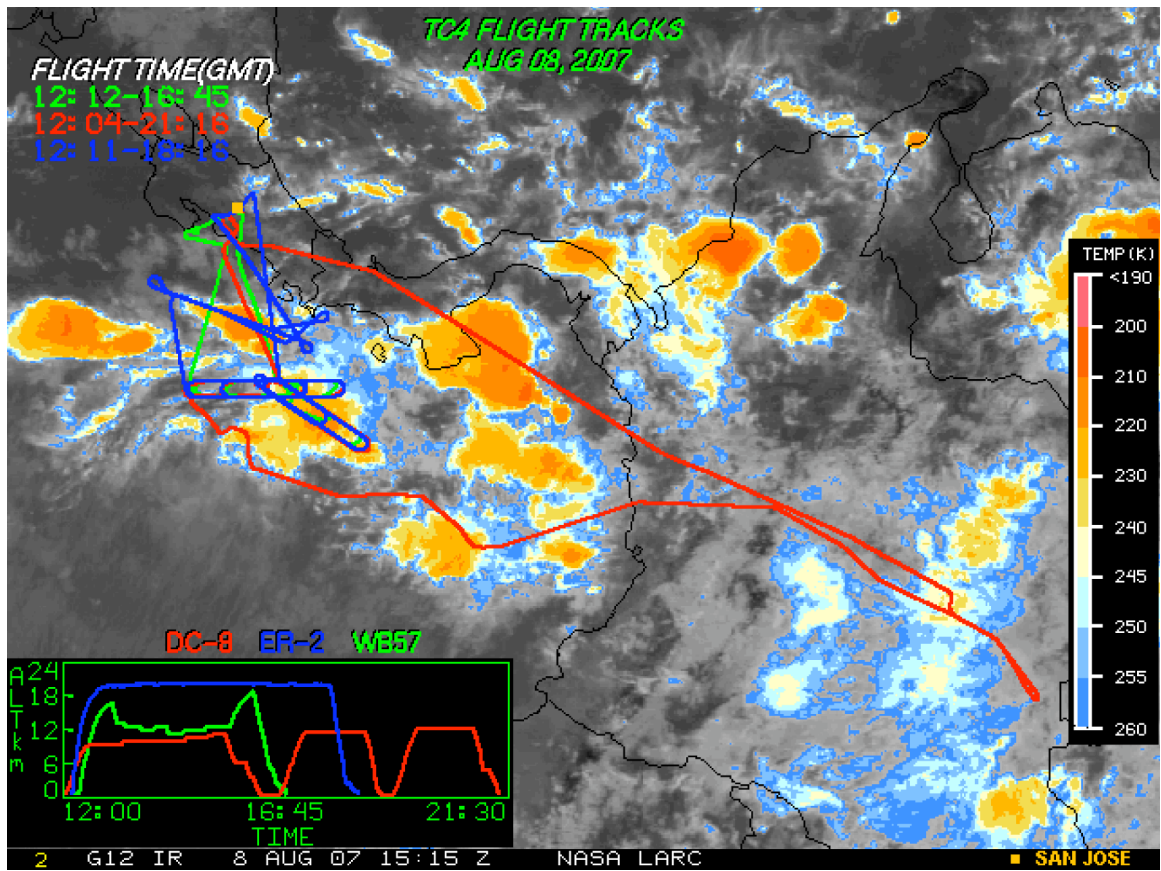


Figure 22. The flight tracks of the DC-8, ER-2 and WB-57F for 8 August, 2007 superimposed on a GOES infrared brightness temperature image. For an explanation of the keys see Figure 8.

http://www-angler.larc.nasa.gov/tc4/flttrks/aug08/ALL_ALL.GOESIR.2007220.1528.gif

1921
1922
1923